Journal of the Optical Society of America B
OPTICAL PHYSICS

Attosecond optics and technology: progress to date and future prospects [Invited]

ZENGHU CHANG,[1,*] PAUL B. CORKUM,[2] AND STEPHEN R. LEONE[3]

[1]Institute for the Frontier of Attosecond Science and Technology, Department of Physics and CREOL, University of Central Florida, Orlando, Florida 32816, USA
[2]Joint Attosecond Science Laboratory, University of Ottawa and National Research Council of Canada, 100 Sussex Drive, Ottawa, Ontario K1A OR6, Canada
[3]Departments of Chemistry and Physics, and Chemical Sciences Division, Lawrence Berkeley National Laboratory, University of California, Berkeley, California 94720, USA
*Corresponding author: Zenghu. Chang@ucf.edu

Received 4 January 2016; revised 3 April 2016; accepted 11 April 2016; posted 12 April 2016 (Doc. ID 256713); published 11 May 2016

The milestones of attosecond optics research in the last 15 years are briefly reviewed, and the latest trends in applications in gaseous and condensed matter are introduced. An outlook on future development of attosecond soft x-ray sources and their application is provided.

OCIS codes: (320.0320) Ultrafast optics; (020.2649) Strong field laser physics; (190.4180) Multiphoton processes.

http://dx.doi.org/10.1364/JOSAB.33.001081

1. INTRODUCTION

A natural time scale of electron dynamics in atoms, molecules, and condensed matter is on the order of attoseconds, 1 as = 10^{-18} s [1]. The production of attosecond optical pulses for observing and controlling electron motion is presently one of the fastest advancing frontiers in ultrafast laser research [2]. The FWHM duration of a Fourier transform-limited Gaussian pulse, τ_p, is related to the frequency width, $\Delta\omega$, by the equation $\tau_p(\text{as}) \approx \frac{1825}{\hbar\Delta\omega(\text{eV})}$ [3]. As an example, the calculated spectrum of a 10 as pulse is shown in Fig. 1, which extends over a broad range of soft x rays. The spectrum of visible and infrared light is not wide enough to support pulses less than 1 fs. Temporally coherent ultraviolet and x-ray wavelengths are needed instead, but such pulses are technically difficult to produce because of the lack of proper broadband laser gain media in this short-wavelength range.

The broadband light required to support attosecond pulses is produced by a process called high-order harmonic generation (HHG), when high-power short-pulse lasers interact with noble gases, a phenomenon discovered in 1987 to 1988 [4,5]. A typical high harmonic spectrum starts with a fast decrease of intensity versus photon energy, followed by a broad plateau that extends to the extreme ultraviolet (XUV) and an abrupt cutoff. The temporal coherence of the XUV light was understood by a three-step semiclassical model and a quantum model at the single atom level [6–9]. The typical intensity on the gas target is on the order of 10^{14} W/cm^2. The corresponding electric field of the linearly polarized light is 10^8 V/cm, which is comparable with the internal Coulomb field in an atom. For instance, the field that the 1s electron in the hydrogen atom experiences is 5.14×10^9 V/cm. In such a strong external field, an electron can be freed from an atom via tunneling ionization. The high-energy photon is produced when the electron accelerated by the intense laser field recombines with the parent ion. This three-step process occurs in one laser cycle. Theories depict that an attosecond burst is emitted when the electron returns to the ground state, and the high harmonic comb is the result of beating of a train of attosecond pulses generated over many laser cycles [10].

Nd:YAG and KrF excimer lasers were used in these pioneering experiments to drive the nonperturbative nonlinear process. In the 1990s, the femtosecond Ti:Sapphire laser was developed and became the workhorse for HHG research [11]. The yield of the high harmonic generation with these lasers is determined by the single atom response and macroscopic phase matching [12]. XUV radiation from atoms at different locations in the partially ionizing gas medium may not add up constructively on the detector due to the difference between the phase velocity of the laser induced polarization and that of the XUV field. Unlike second- or third-harmonic generation in crystals, phase matching cannot be achieved by making use of the birefringence of the nonlinear medium, as gases are isotropic. Interestingly, the strong field/Lewenstein model predicts that the phase of the dipole moment responsible for a particular harmonic depends on the driving laser intensity [13], which is not the case for low-order perturbative harmonic generation. This effect plays an important role in phase-matching high-harmonic generation because of the variation of the laser intensity in transverse/propagation directions. This is the reason that gas cells in high

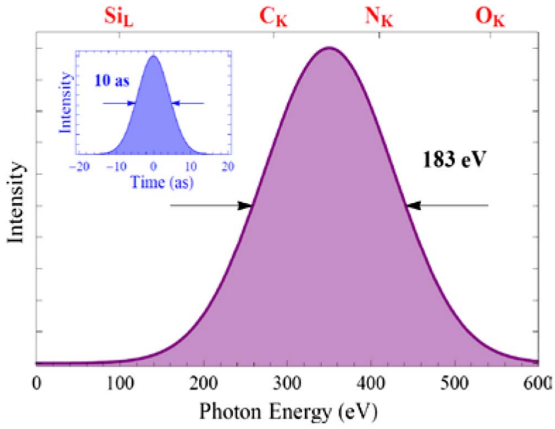

Fig. 1. Spectrum of 10 as transform-limited Gaussian pulses. The photon energies of x-ray emission lines from several elements are labeled.

harmonic generation experiments are often positioned after the laser focus. The change of index of refraction induced by ionization can also be balanced by neutral atoms [14]. The cutoff photon energy, and thus the total high harmonic spectral span, is determined by the maximum kinetic energy that an electron gains from the driving laser field and the phase-matching bandwidth.

In 2001, attosecond light pulse characterization in HHG was demonstrated for the first time [15,16]. Because the power spectrum could be easily measured, the main task was to determine the spectral phase. Due to the low efficiency of high-order harmonic generation processes, which is on the order of 10^{-6}, the energies of the attosecond pulses are on the order of picojoules to nanojoules [17]. The low intensity makes it difficult to implement the phase retrieval techniques developed for femtosecond lasers that rely on nonlinear optical gating processes. Novel schemes were developed to characterize a train of attosecond bursts and single isolated attosecond pulses, which retrieve the phase by analyzing the photoelectron spectrum emitted from atoms bathed in a combination of XUV and strong near-infrared (NIR) laser fields. The photoelectron is emitted when an atom absorbs an XUV photon and one or more NIR photons simultaneously, which serves as the nonstationary time filter required for fully characterizing the optical pulses.

Significant progress in the generation and characterization of attosecond pulses has been made in the last 15 years. The shortest pulses, 67 as, were achieved in 2012 [18], which were characterized by two different phase retrieval methods, frequency-resolved optical gating for complete reconstruction of attosecond bursts (FROG-CRAB) and phase retrieval by omega oscillation filtering (PROOF) [19,20]. Recently, high harmonic generation in solids has also been demonstrated [21]. In addition, attosecond pulse usage has dramatically increased in solving scientific problems [22], already resulting in hundreds of publications describing completed and proposed experiments and corresponding theory. In this short overview, the latest efforts in reducing the pulse durations, increasing the pulse energies, and increasing the photon energies are introduced. Innovative *in situ* pulse characterization schemes for studying HHG from both gas and solid targets are illustrated. Brief descriptions of a few exciting results from attosecond applications are given, followed by a perspective on the future of the attosecond field.

2. NEXT-GENERATION DRIVING LASERS FOR ATTOSECOND GENERATION

A. Carrier-Envelope Phase-Locked 100 TW-Level Lasers

The success of the first-generation attosecond light sources is built upon high-power femtosecond Ti:Sapphire technology [23]. The Ti^{3+} ions that replace the Al atoms in the Al_2O_3 crystal exhibit a large simulated emission cross section in the broad spectral range from 650 to 1100 nm. Ti: Sapphire can be conveniently pumped by the second harmonic of Nd doped YAG, YLF, and other host media. In the last decade, arc lamps and flash lamps in these pump lasers have been replaced by laser diodes, which leads to user-friendly products that deliver either single-longitudinal mode beams for pumping laser oscillators or laser pulses with high energy, high repletion rate, and excellent pulse-to-pulse stability for pumping amplifiers.

The combination of the ultrabroad gain bandwidth of Ti:Sapphire and the Kerr-lens mode-locking technique results in laser oscillators that routinely produce nanojoule pulses with less than 10 fs duration and ~80 MHz repetition rate. The pulses can be amplified to a few mJ or higher by chirped pulse amplification (CPA) that operates at ~1 kHz. The femtosecond pulses from an oscillator are stretched to several hundred picoseconds in a grating compressor to reduce the intensity and avoid damage of the amplifier gain media. The amplified pulses are then compressed back to femtoseconds by a pair of diffraction gratings or prisms. The typical gain of the amplifiers is on the order of 10^6 or higher, centered at 800 nm. The gain narrowing effects broaden the pulses to ~25 fs.

Various subcycle gating schemes have been developed to generate isolated attosecond pulses for pump–probe experiments [2], which will be introduced in Section 3. For some gating methods such as double optical gating, the shorter the driving laser pulses, the higher the conversion efficiency [24]. This is because only the energy within one laser cycle can be converted to a single attosecond pulse. Therefore, the 25 fs pulses are compressed by coupling the laser to a noble gas-filled hollow-core fiber. The self-phase modulation in the fiber broadens the spectrum by a factor of 5 or more. Afterward, the positive chirp of the pulses is removed by several pairs of mirrors with negative group delay dispersion, and the pulse duration can reach 5 fs or shorter. The typical pulse energy is ~1 mJ [25]. The kHz Ti:Sapphire laser system at the Institute for the Frontier of Attosecond Science and Technology is shown in Fig. 2.

The electric field of a transform-limited Gaussian pulse can be expressed by $\mathcal{E}(t) = E_0 e^{-2\ln 2(\frac{t}{\tau_p})^2}\cos(\omega_0 t + \varphi_{CE})$, where E_0 and ω_0 are the peak amplitude and center angular frequency, respectively. The carrier-envelope (CE) phase, φ_{CE}, measures the offset between the peak of the pulse envelope and the maximum of the field oscillation, as illustrated in Fig. 3 [3]. As described in Section 3, several gating schemes

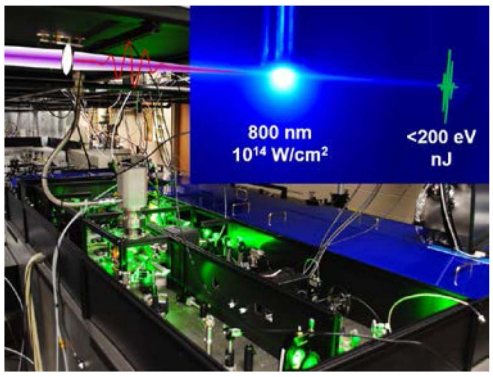

Fig. 2. Ti:Sapphire laser for driving the first-generation attosecond light sources.

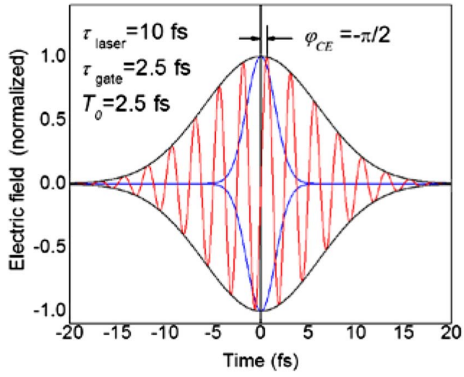

Fig. 3. Carrier-envelope phase, which becomes important when the gating (blue online) approaches a laser cycle, T_0. Republished with permission of Taylor & Francis, from [3].

have been developed for generating isolated attosecond pulses, and the carrier-envelope (CE) phase of the driving laser plays an important role. The CE phase of a femtosecond oscillator can be stabilized by using the *f-to-2f* technique developed for optical frequency metrology [26]. Various schemes have been implemented to lock and control the CE phase of kHz femtosecond amplifiers. It was demonstrated that one of the main sources of CE phase drift in a Chirped Pulse Amplifier is the variation of the spacing between the gratings in the stretcher and compressor [27]. By feedback controlling the grating position, the CE phase of the amplified pulses can be locked to ~100 mrad RMS, which satisfies the requirements for isolated attosecond pulse generation [28].

The peak intensity at the focal point of a Gaussian beam can be estimated by $I_0 = \frac{1.88\epsilon_p}{\tau_p \pi w_0^2}$, where w_0 is $1/e^2$ radius of the focal spot. The energy of the attosecond pulse, ϵ_p, generated with a kHz Ti:Sapphire laser is on the order of picojoules to nanojoules, which is determined by the limited output energy of the hollow-core fiber (~1 mJ) and the conversion efficiency from NIR to XUV (~10^{-6}). The intensity that can be reached by a 200 as, 1 nJ pulsed XUV beam focused to a 10 μm spot is 3×10^{12} W/cm^2. To perform attosecond-pump attosecond-probe experiments, which are essentially second-order XUV nonlinear optics experimenta, 10^{14} W/cm^2 is required [29,30]. Considering the losses in beam transporting, filtering and focusing, microjoule level attosecond pulses need to be produced from the generation target.

Femtosecond lasers with ~0.1 to 1 J level pulse energy are being developed to significantly increase the attosecond pulse energy [31,32]. Although lasers with such energy are available for relativistic plasma physics research, their CE phase is not locked, and the pulse width is too long for generating isolated attosecond pulses with high conversion efficiency. The high energies in these lasers are achieved by amplifying the sub-10 fs, nJ pulses from the oscillator in a CPA chain with a total gain of 10^9 or higher. Gain narrowing limits the pulse width to ~30 fs. A double CPA approach has been taken to minimize the effects of gain narrowing, as shown in Fig. 4 [33].

The first CPA is similar to the one shown in Fig. 2, which runs at 1 kHz and produces 1 mJ pulses with a bandwidth supporting 5 fs pulses. Therefore, the gain narrowing in this CPA stage is compensated by the spectral broadening in the gas-filled hollow-core fiber. The output of the fiber serves as the seed for the second CPA, which has a moderate gain of ~1000. In addition, spectral filters with higher loss at the peak of the gain cross-section curve and lower loss at the wings of the amplified spectrum are added to further compensate the gain narrowing. After correcting for the spectral phase errors, 14 fs pulses with 350 mJ energy were generated at 10 Hz. With this laser, a 100 nJ extreme ultraviolet pulse that can support 230 as isolated attosecond pulses at 35 eV was generated from argon gas using the generalized double optical gating technique [34,35].

The low repetition rate of the joule level laser poses a challenge for locking the CE phase. Direct implementation of the feedback control methods developed for kHz lasers is not feasible because the 10 Hz *f-to-2f* signal that measures the phase variation is not fast enough to compensate for the rapid frequency components of the phase drift that can extend to ~100 Hz. A fast CE phase probing scheme was demonstrated to solve the problem [33]. The kHz pulses from the first CPA were sent to the second CPA without amplification to monitor the CE phase variation at ~1 kHz rate, which is used as the feedback control signal to stabilize the CE phase of the final output, as depicted in Fig. 4. With this scheme, the effects of CE phase on the XUV spectrum generated with the 10 Hz laser are observed, as shown in Fig. 5.

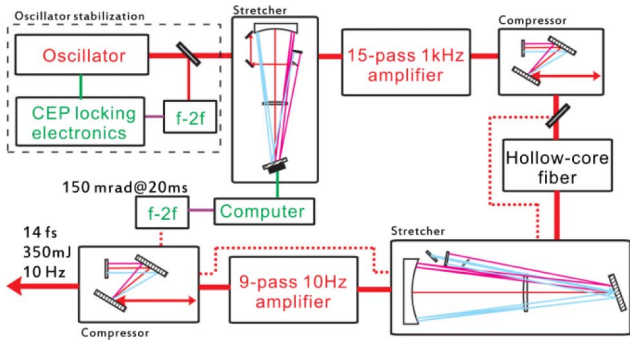

Fig. 4. Double chirped pulse amplification for generating Joule level pulses with <15 fs duration. Reproduced from [33], with the permission of AIP Publishing.

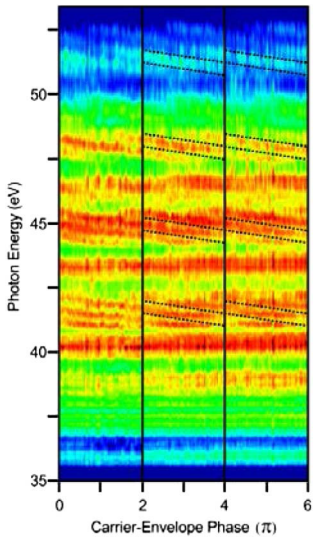

Fig. 5. Effects of CE phase on the XUV spectrum generated with a 10 Hz laser. Reproduced from [33], with the permission of AIP Publishing.

Another approach has been demonstrated to achieve 5 fs pulses with 80 mJ pulse energy at 800 nm and 10 Hz [36], which is based on optical parametric chirped pulse amplification (OPCPA), discussed in the next section. Comparing to CPA, the gain bandwidth of OPCPA is much broader. The main difficulty is the lack of commercially available pump lasers with the required pulse duration and synchronization with the seed pulses.

B. Few-Cycle, High-Power Mid-Infrared Lasers

The measured sub-100 attosecond pulses so far cover a spectral range of 55–130 eV [2]. For atomic physics, condensed matter, and chemical and atomic application, it is important to extend the attosecond spectrum to the "water window," i.e., the photon energy range from 280 to 530 eV, which is within the range shown in Fig. 1. Such soft-ray sources make it possible to use core-level transitions to study electron dynamics in materials containing carbon, nitrogen, oxygen, and several other key elements. Although subcycle gating of the high harmonic generation process has yielded an x-ray supercontinuum extending to 600 eV [37], the photon flux is too low for attosecond pulse characterization and applications.

In 2001, it was demonstrated experimentally that the cutoff photon energy of high-order harmonic generation can be dramatically increased when the center wavelength of the driving lasers is longer than that of Ti:Sapphire [38]. The mechanism can be explained by the semi-classical model that describes the generation of an attosecond burst during one driving laser cycle in three steps. First, an electron is released by tunneling through the potential barrier formed by the atomic Coulomb field and the driving laser field. Then, the freed electron gains kinetic energy while being accelerated by the electric field of the laser. Finally, the electron returns to its birth place, recombines with the parent ion, and emits a photon. The photon energy is equal to the binding energy of the atom plus the kinetic energy of the returning electron [6,7].

It turns out that the ionization rate of an atom in intense laser fields does not depend much on the laser wavelength. Therefore, the highest intensity an atom can experience before being fully ionized is almost wavelength independent. This intensity is called the saturation ionization intensity, I_s. On the other hand, the energy gain of an electron in an electric field scales quadratically with the acceleration time or the laser cycle/wavelength. For a given driving laser pulse duration, the maximum energy of the photon emitted by the atom is given by $\hbar\omega_c(\mathrm{eV}) = I_p(\mathrm{eV}) + 3\times10^{-13} I_s\left(\frac{W}{\mathrm{cm}^2}\right)\lambda_0^2(\mu\mathrm{m}^2)$, or [39]

$$\hbar\omega_c = I_P + \frac{0.5 I_p^{3.5}\lambda^2}{\left[\ln\left(\frac{0.86 I_p 3^{2n^*-1} G_{lm} C^2_{n^*l^*}}{-\ln(1-p_s)}\tau_p\right)\right]^2}, \tag{1}$$

where p_S is the ionization probability at the peak of the driving laser pulse that defines the saturation of the ionization of the ground state population, which can be set to 0.98. The unit of $\hbar\omega_c$ and I_P is eV. The unit of λ is μm. τ_p is in fs. The values of n^*, G_{lm}, and $C^2_{n^*l^*}$ associated with the quantum parameters of the ground state are found in [3]. Equation (1) shows the explicit dependence of the cutoff photon energy on the driving laser wavelength.

Figure 6 shows the calculated photon energy that can potentially be reached with noble gases for different laser wavelengths using Eq. (1). The pulse duration of the driving laser was fixed at 25 fs in the single atom calculations. When 1D phase-matching is considered, p_S can be replaced by the ionization probability, p_{pm}, at which the index of refraction of the remaining unionized gas equals to that of the plasmas formed by the ionized portion of the gas, which leads to

$$\hbar\omega_{c,pm} = I_P + \frac{0.5 I_p^{3.5}\lambda^2}{\left[\ln\left(\frac{0.86 I_p 3^{2n^*-1} G_{lm} C^2_{n^*l^*}}{-\ln(1-p_{pm})}\tau_p\right)\right]^2}. \tag{2}$$

The values of p_{pm} can also be found in [3]. For helium, p_{pm} equals to 5×10^{-3}, which is much less than p_S. Therefore the cutoff photon energy under such a phase-matched condition is less than that from a single atom calculation.

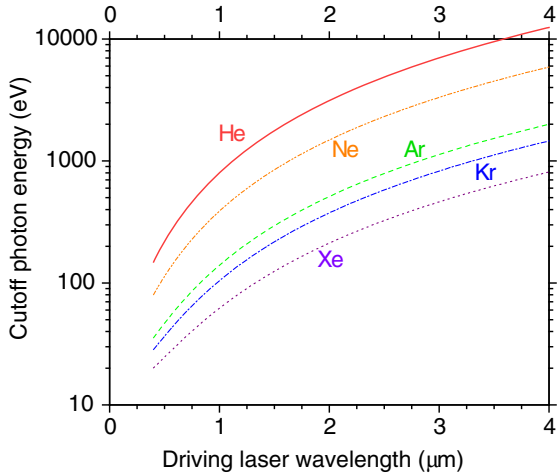

Fig. 6. Calculated maximum photon energy as a function of driving laser wavelength. Republished with permission of Taylor & Francis, from [3].

The first demonstration of high harmonic cutoff extension with long-wavelength lasers was conducted by using an optical parametric amplifier (OPA) pumped by a femtosecond Ti:Sapphire laser. The nonlinear crystal is BBO. The energy of the 1.5 μm pulses was less than 100 μJ. Later, higher-energy OPAs, >1 mJ, ~45 fs, became commercially available. When the OPA output beam is coupled to a gas-filled hollow-core fiber and the positive chirp of the output pulse is compensated by the negative group velocity dispersion of fused silica, two-cycle pulses with 0.5 mJ or more energy centered at 1.8 μm were produced [40]. When the laser is focused on a neon target, the high harmonic spectrum covers the range of 160 to 400 eV, as shown in Fig. 7 [41]. Isolated attosecond bursts have also been generated by using the attosecond lighthouse technique described in Section 3 [42].

To further increase the driving laser energy and avoid the 50% loss of the hollow-core fiber, optical parametric chirped pulse amplifiers with kHz repetition rate, two-cycle duration, and more than 1 mJ energy have been developed at 1.6 to 2 μm center wavelengths. A typical OPCPA is shown in Fig. 8, which takes advantage of the matured Ti:Sapphire laser technology [43,44]. The carrier-envelope phase stabilized seed pulses with ~100 nJ energy are produced by a difference frequency-generation process driven by the mJ level white light from a gas cell or a gas-filled hollow-core fiber. The nonlinear crystals for parametric amplification are BiB_3O_6, which can be phase-matched over a very broad spectral range from 1.2 to 2.3 μm when pumped by Ti:Sapphire lasers. The final pulse energy has reached 3 mJ [45]. The CE phase effects of "water window" x-ray generation with such lasers have been demonstrated.

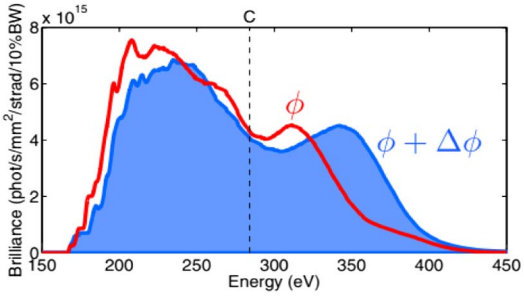

Fig. 7. Soft x-ray spectrum generated by CE phase stabilized OPA laser [41]. Reprinted with permission from Optical Society of America.

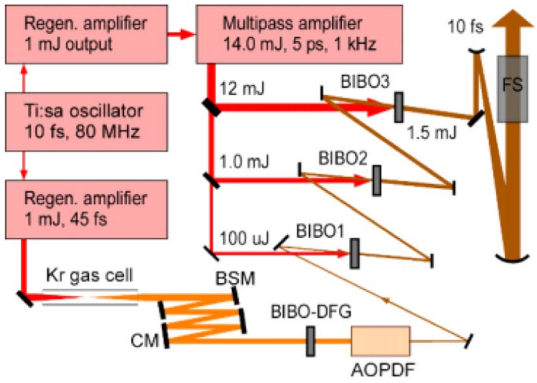

Fig. 8. Two-cycle OPCPA laser at 1.6 μm pumped by Ti:Sapphire lasers [44]. Reprinted with permission from Optical Society of America.

Other OPCPA pump lasers such as Yb:YAG operating at 1.03 μm have been developed [46,47]. The pump energy at 1 kHz may be 100 mJ or higher, which paves the way for generating two-cycle lasers at 2 μm with more than 10 mJ energy. It is known that, when the driving laser wavelength is increased, the single atom response rapidly reduces as a result of the quantum diffusion of the ionized electron wave packet [38]. By filling an ~1 mm long cell with high-pressure (3.5 Bar) neon gas, the x-ray flux at 300 eV generated with a two-cycle, one kHz, 1.85 μm laser is reached at 10^7 photons/s/1% bandwidth [41]. Therefore, improving macroscopic phase matching in high-pressure gases [48] and increasing the driving laser energy as well as repetition rate is critical for wide applications of "water window" attosecond x-ray pulses.

3. NOVEL ATTOSECOND GATING AND CHARACTERIZING ATTOSECOND PULSES

During multiphoton ionization, many things occur. The newly freed electron may elastically scatter, inelastic scatter, and emit incoherent light, but, in Fig. 9, we concentrate only on that aspect of strong field atomic physics that leads to high harmonic and attosecond pulse generation. In Fig. 9, the dynamics of the process are represented by the orange arrow. The two essential components of the electron wave function are captured: one bound by the Coulomb potential of the ion and the other, an electron wave packet tunneling from the atom and moving in the continuum with a semi-classical motion. The total wave function is the sum of the two parts, and the illustration captures the overlap of the two components of the wave function. The charge oscillation due to this laser-induced interference is responsible for attosecond pulse generation. In other words, attosecond pulse generation can be thought of as an interference process.

Before discussing attosecond gating and characterization, it is useful to introduce the concept of quantum trajectories for the ionizing electron. A quantum trajectory is a semiclassical mapping of a moment of birth into a moment and energy of re-collision. The set of quantum trajectory is the electron re-collision wave packet, as illustrated in Fig. 9. In the high harmonics context, quantum trajectories have their origin in the "Lewenstein model" of high harmonic generation [8]. In the approximation where we ignore the ionic potential along the quantum trajectory (known as the strong field approximation),

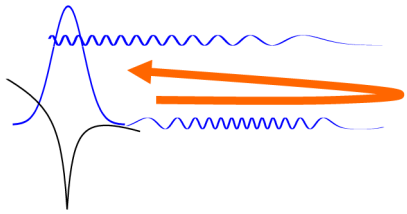

Fig. 9. Illustration of the electron wave packet that separates from the bound state of an atom, molecule or solid near a field crest but re-collides after motion in the continuum. Quantum trajectories link moments of birth in the wave packet to time and energy of re-collision.

and we use classical physics to estimate the path, then any moment of birth during the quarter period following a field crest would return the electron to its origin. This means that, averaged over one half-cycle, 50% of the wave packet has the potential to re-collide within one period of birth [6], converting its kinetic and potential energy into a photon.

Phase distinguishes coherent from incoherent optics, so phase control is a tremendously important variable. As the electron transits the quantum trajectory, it accumulates phase with respect to the wave function from which it originated. The phase is essentially determined by the classical action of an electron along the trajectory plus a contribution from the ionization potential of the state from which the electron originated [8]. Thus, the radiation that is created when components of the electron wave packet recombines to its initial state (or any other phase related state) and has a phase that we can estimate with classical physics or measure through analyzing the emitted radiation. Because we can manipulate the classical action by means of the field, we can control the phase of the XUV radiation. Alternatively, measuring the phase of the XUV light tells us about the manipulation.

While we have spoken of an atom, there is nothing specific about the ideas that confine us to atomic media. Small molecules are much like atoms in the context of this discussion [49], and large molecules or wide bandgap semiconductors allow a similar response if we map the idea of ionization onto electron-hole pair creation [50]. Thus, the form of extreme nonlinear optics that has just been discussed, although not unique [51,52], is relatively general.

With both mid-infrared and 800 nm wavelength drivers in mind, consider now the re-collision. The key to producing isolated attosecond pulses is to ensure that no trajectories other than those that originate in one quarter-field cycle of the fundamental pulse are able to produce radiation in the direction that is observed. If this is fulfilled, then the resulting radiation is confined to a time determined by the classical trajectories, thus a time window of approximately 50% of the light period. For 800 nm light, this would be about 1.5 fs.

To progress further, now consider the phase coherence across a beam. As previously discussed, a moment of birth is mapped into a moment and energy of re-collision. For a given energy of re-collision (or XUV wavelength), this mapping depends on the wavelength and field strength of the fundamental. In a realistic beam with a spatial intensity profile, the field strength depends on the spatial position of the atom in the laser focus. Therefore, across the wavefront the radiation is produced with different phases.

The classical mapping of moment of birth into energy of re-collision suggests that it is useful to subdivide the quarter period after any field crest into two times that generate the same frequency. Electrons are born soon after the field crest and returning between three-quarters period to one period later. They are the "long trajectory electrons." They produce radiation with a characteristic spatial phase. There are also electrons born later and returning earlier. These short trajectory electrons produce XUV radiation that has a different spatial phase structure.

The differing spatial phase of the radiation created by short and long trajectory electrons across the beam profile means that the long and short trajectory components of the beam separate in the far field and one or the other can be observed, usually the short trajectory contribution.

Radiation produced by the short trajectory electrons begin with the longest wavelength component arriving earliest, and the output is frequency chirped over the next ~ quarter period of the fundamental, until it reaches the cutoff (or maximum) frequency permitted for this intensity and wavelength driver. A linear chirp, such as this, can be removed by passing the pulse through a dispersive material [53]. In this way, we reach shortest controlled pulse ever produced: 67 as [18].

With high-energy infrared drivers, such as those previously described, the phase accumulated along any electron trajectory is greater, as is the divergence difference between radiation originating from the short and long trajectory. The attosecond pulses they create will have a higher cutoff energy and the greater the bandwidth but a smaller chirp [54]. Photon energies in the keV range are possible [48], and pulse durations near 10 as seem feasible. Therefore, we now consider methods for generating isolated attosecond pulses.

A. Subcycle Gating in Gases and Solids

For isolated attosecond pulse generation, there is one overreaching requirement. As discussed above, the fundamental pulse must be carrier-envelope-phase stable. Once this is achieved, there are two general methods for selecting an isolated attosecond pulse from the train of pulses that constitutes the high harmonics. One approach is to manipulate the re-collision electron so that only radiation from one re-collision is important. This approach operates on the single-atom level. That is, each atom in the gas of atoms creates an identical attosecond pulse. The pulse measured in an experiment is the coherent sum of all of these atomic-level attosecond pulses. The other approach is to manipulate the beam so that only radiation from a single re-collision can be emitted in a given direction. Any atom in the focal volume will now create a train of pulses, but, like a phased array, the radiation is directed to a slightly different direction on each half cycle of the fundamental. In this case, attosecond pulse selection operates at the level of the wavefront of the beam.

1. Amplitude Gating

The first isolated attosecond pulses were generated with the first of the two methods mentioned above [16]. Specifically, the method is called "amplitude gating." For amplitude gating, the gate operates on the dual requirement that the field must be high enough to ionize the atom at one field crest *and that it must remain strong enough to force an energetic re-collision* ~2/3 *of a period later*. If the former is not fulfilled, then there is no re-collision by definition. If the latter is not fulfilled, then the radiation created in the re-collision and recombination can be removed with a high photon energy bandpass filter. For a short enough driver pulse, there is only one re-collision that fulfills this dual requirement.

2. Polarization Gating

The first proposed active gating method was polarization gating [55]. Polarization gating also falls within the first category above. It seeks to ensure that the electron and ion will miss

each other when they are given an opportunity to re-collide except for only one half-period. Polarization gating achieves this requirement by using a fundamental pulse with time-dependent elliptical polarization. As shown in Fig. 10, it can be achieved by time-delayed pulses with opposite handed circular polarization. These pulses can be created passively with wave plates [56]. The result is a short driving pulse continuously changes from circular to linear and then back to circular of the other handedness. When a gas is illuminated with such a pulse, high harmonic radiation can only be emitted for a brief interval when the driving field is near linear. (This can be readily confirmed with a classical trajectory calculation.) Thus, the emission is confined to a fraction of the pulse duration, which can be just a fraction of an optical cycle.

3. Attosecond Lighthouse

There are many variants of polarization gating, such as double optical [57] or partial polarization gating [58], but rather than deal with them in detail, consider the second general approach to attosecond pulse selection. It has already been discussed how the short and long trajectory electrons create radiation with different divergences, allowing the long and short trajectory contribution to be isolated in the far field. One might ask if there is another beam structure that will do even better. The answer is "yes." Imagine a space–time coupled beam that has a time-dependent wavefront, a wave front that changes directions continuously throughout the beam. Then, radiation created each half cycle will propagate in a different direction. If that difference exceeds the beam divergence, then, as the beam propagates, the spatially overlapping attosecond pulse train of the high harmonics separates in the far field into isolated attosecond pulses. This method, known as the "attosecond lighthouse" [59,60], is illustrated in Fig. 11. It creates multiple isolated attosecond pulses, and each one of them is coherent with the others and potentially individually controllable. They will prove a powerful resource for measuring attosecond dynamics.

B. Characterization of Attosecond Pulses

Now consider attosecond pulse measurement. One's initial tendency is to try to directly adapt laser methods of

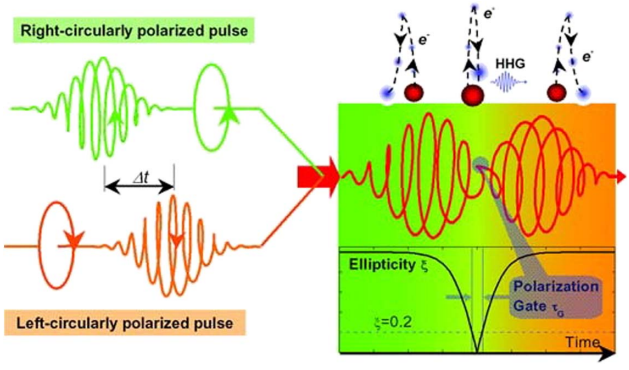

Fig. 10. Illustration of polarization gating. Left and right circular polarized beams are combined to produce a fundamental beam with time-dependent polarization. Re-collision and, therefore, harmonic generation are only possible during a brief interval when the polarization is near linear. Republished with permission of Taylor & Francis, from [56].

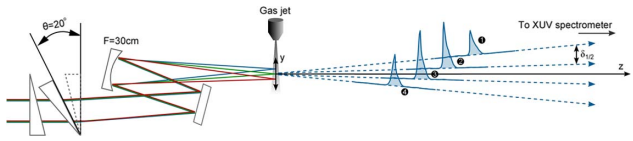

Fig. 11. Taken from [59] showing a diffraction-limited few-cycle pulse passing through two complementary wedges that are slightly unbalanced (equivalent to a very small angle wedge). In the far field, the beam has a time-dependent wavefront. High harmonics produced with such a pulse break into isolated pulses that propagate in slightly different directions. These many phase-related attosecond beams can be independently controlled.

autocorrelation, spectral phase interferometry for direct electric-field reconstruction (SPIDER) or FROG to attosecond pulse measurement. However, this turns out to be difficult, if not impossible. Primarily the attosecond pulses are too weak, and there is not an efficient enough nonlinear material. Instead, the adaptation of other methods is general considering the clear relationship between key elements of laser and attosecond methods.

A short pulse only exists because of the phase relation between the different frequencies that make up the pulse. Therefore, any measurement needs a method to directly or indirectly compare the phase at different frequencies. In all cases, this is achieved using a nonlinear process to shift radiation from one frequency to another. For laser pulses, many materials are effective nonlinear media. In attosecond technology, an ionizing (or recombining) electron can play the same role. For laser pulses, a beam splitter divides the beam in question into two components. In attosecond technology, the nonlinearity arises from mixing one or more infrared photons with the attosecond ionizing (or recombining) electron.

Two basic technologies are used to measure attosecond duration pulses. For both, the electron is the key element that allows measurement because the electron is so sensitive to fields. In one approach, we exploit the streak camera idea. In its attosecond incarnation, we transfer amplitude and phase information of the attosecond pulse to a photoelectron replica and then measure the photoelectron replica by mixing in the energy and phase structure of one (or more) infrared photons [61]. In the second approach we use the ionizing atomic gas in which the attosecond pulse is being used as the highly nonlinear medium that permits measurement. Here, it is the antenna-like nature of the re-collision electron that allows us to encode information onto the attosecond pulse itself. The pulse then contains information on its own duration, and the pulse duration information can be retrieved using FROG-like methods.

1. Streaking

Consider streaking first. Photoionization is a coherent process. During photoionization, the amplitude and phase of a light pulse are transferred to an electron through the transition moment. For simple atoms, the transition moment is well understood and, therefore, a photo-electron measurement can serve as a proxy for measuring the amplitude and phase of the pulse itself. This is the fundamental idea underlying the method called "reconstruction of attosecond harmonic beating by

interference of two-photon transitions" (RABBITT) [15], PROOF [20], and attosecond streaking [62,63]. Here, the nonlinearity arises from mixing in one or more infrared photons. In PROOF and RABBITT, one infrared photon that is added; for attosecond streaking, many are added.

Attosecond streaking (sketched in Fig. 12) can be understood classically [64]. While an electron is bound, it cannot respond to the infrared laser field. However, as soon as the electron is released, it is accelerated by the field of the laser. Thus, the electron gains energy from the XUV photon and also from the integral of the time-dependent field from its moment of ionization to its moment of re-collision. The laser field's contribution to the electron's energy depends on the range of moments of birth—*or the pulse duration*.

The strength of streaking methods is that the attosecond pulse can be created, filtered, and transported to an experiment before it is measured. As long as the atomic system in which the measurement is made is well understood, the pulse is accurately measured where it is used. The weaknesses of the method are twofold: (1) an attosecond pulse is space–time coupled. If the source is reimaged into the medium (as is usually the case) and the IR field overlaps the full image, then streaking measures the spatially averaged pulse; (2) because the photoionization cross section decreases with photon energy, streaking-related measurement methods become increasingly difficult, as interest moves to attosecond pulses with higher photon energy and potentially shorter pulses.

2. In situ Measurement

In situ methods [64] share some aspects of streaking. Both rely on photoelectrons, but for *in situ* measurement, the photoelectron that is responsible for the measurement is the re-collision electron itself. When the re-collision electron photo-recombines, it creates the attosecond pulse as a photon replica of itself as seen through the transition moment. That is, attosecond pulse generation is the inverse of photoionization. As with streaking, the job is to measure the (photo-recombining) electron's spectral phase.

In common with PROOF or RABBITT, for *in situ* measurement a weak control field is used to perturb the trajectory of the re-collision electron, modifying its phase. Modification is only possible during the brief interval between birth and re-collision. Using a perturbing field incident at an angle

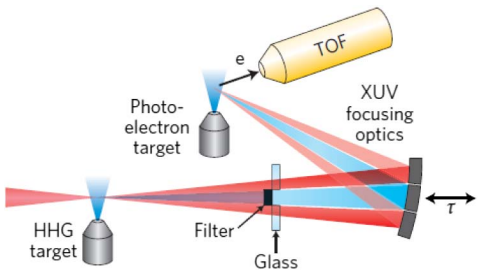

Fig. 12. Sketch taken from [64] of an attosecond streak camera, showing the source jet, labeled the HHG target and the measurement jet, labeled the photoelectron target. Streaking is performed with the fundamental beam (red) separated from the attosecond pulse (blue) by a filter.

produces a modification to the phase of the re-collision electron wave packet, which varies as the detection is translated across the attosecond pulse wavefront. In this way, a spatial modulation can be induced on the attosecond pulse. If the angle is small, then the attosecond beam is deflected with the deflection depending on the relative phase between the perturbing beam and the attosecond pulse. If the angle is large, then the deflecting beam is diffracted. In both cases, information that is imposed on the electron wave packet is transferred to the XUV radiation where it is "read."

With the beam profile depending on the phase (or time) the 2D information is obtained for reconstructing the beam *spatial profile at each frequency*. This is very much like how FROG determines the time profile of a short pulse from the spectral profile as a function of time. The phase of the time-dependent deflection of the beam for each frequency component, relative to the beam deflection at some reference frequency, determines the spectral phase at the associated frequency [65].

The strength of *in situ* measurement is that the space–time structure of an attosecond pulse is obtained, and the measurement process is so efficient that it allows single-shot measurement of the pulse [66] and of the perturbing field [67]. It seems perfectly scalable to high-energy soft x rays and to pulses that are much shorter than those currently produced. The weakness is that the pulse is measured in the medium in which it is created. If the pulse is filtered afterward, these changes require that the modified beam is measured relative to the just measured pulse by spectral interferometry.

C. Controlling Attosecond Pulses

Measurement and control are deeply entwined ideas. An unknown pulse is measured by controlling the final state of an observable. Measuring an unknown pulse requires a material with a well-understood response so that the changes in the final state can be understood. The same set of steps can determine (1) the unknown response of a material if the pulse is well-determined; (2) it can control the observable, should we be interested in its control. Therefore, all methods of measuring attosecond pulses can be turned into methods of measuring material response or controlling materials. This is true for both attosecond streaking and *in situ* measurement.

1. Controlling Attosecond Beams

In the case of streaking, we are not so interested in controlling the electron characteristics, although this can lead to new ways to create a laser in the air [68]. The significance of control is much clearer in the case of *in situ* measurement because, here, the information that is needed for measurement is transferred to the optical pulse, thereby modifying the pulse or controlling the pulse. This modification can be quite important and quite dramatic. For example, it is possible to control re-collision on a subcycle basis with a control beam that is perpendicularly polarized. This opens the opportunity to tune an attosecond pulse.

Many control methods are spectrally selective. For example, it is possible to impose spin angular momentum on a beam [69] by mixing two circularly polarized fundamental beams, one the second harmonic of the other, and with different handedness. In this case, the electron re-collision is modulated in such a manner as to create rotating polarization for any emitted

harmonic. Harmonics alternate between left-handed circular; right-handed circular; and absent throughout the full output spectrum.

It is also possible to impose orbital angular momentum on a high harmonic pulse [70–72]. One method is similar to what is done with visible lasers. In laser technology, one writes a phase structure on the beam. In the case of XUV light, the phase structure is written on the re-collision electron by a weak control pulse, and then it is transferred to the XUV light as the electron recombines.

In fact, any phase can be imposed on the XUV beam, as it is being produced via an external control beam adding phase to the re-collision electron along its trajectory. Specifically, this includes a Fresnel zone plate to focus the XUV radiation [73], offering the potential to focus beams that have been just created or to spectrally filter the beam.

2. Transient Grating Spectroscopy

Before concluding this section, it is important return to measurement. Writing grating structures into a medium is closely related to transient grating spectroscopy and 2D spectroscopy: two of the most powerful probing methods used in conventional ultrafast optics. In transient grating spectroscopy, a grating is introduced into the material in order to measure material dynamics, not to control the radiation—although it does both. As shown in Fig. 13, a grating can be induced by a pair of excitation pulses. In transient grating spectroscopy, we aim to follow the materials response as a function of time delay. Transient grating spectroscopy is powerful because the probe pulse is diffracted to a region where it would not otherwise be so the dynamics is observed without background. In fact, one can observe the deflected beam and the diffracted radiation.

Transient grating spectroscopy has been applied to measuring conical intersection dynamics [74] and also photochemical decomposition [75]. In these cases, the pump pulse creates a photoexcitation grating in the molecular gas. As the molecule undergoes its natural dynamics, the excited state grating evolves. As shown in Fig. 13, the probe pulse can be a fundamental beam creating high harmonics (or attosecond pulses) *in situ*. Equally interesting is the case where the probe pulse is an attosecond pulse itself, but that brings us to transient absorption spectroscopy, the subject of the next section of this review.

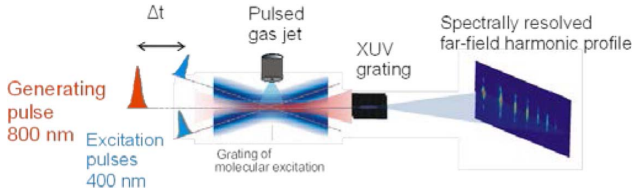

Fig. 13. Adapted from [75]. Reprinted with permission from AAAS. A beam of NO_2 molecules is ejected into the vacuum. Excited by 400 nm light, the NO_2 molecules bend toward a conical intersection. High harmonic radiation created by a delayed, intense 800 nm beam is diffracted by the patterned medium. A fully coherent spectroscopy, the diffraction pattern encodes the time dependence of the amplitude and phase of the transition moment of the excited state relative to the fixed ground state of the molecule.

4. FAST EXPANSION OF SCIENTIFIC APPLICATIONS WITH ATTOSECOND PULSES

Soon after their first demonstration, attosecond pulses were used to measure the lifetime of Auger decay processes [76]. Since then, some experiments have been carried out with attosecond pulse trains, while others have utilized isolated attosecond pulses. In all cases, due to the rather low flux of attosecond pulses, the experiments combine attosecond extreme ultraviolet pulses with few-cycle near-infrared pulses to achieve time measurements.

A. Experimental Methodology

A few key methods have been developed to measure attosecond time-resolved processes. The first is a combination of an isolated attosecond pulse with a carrier-envelope-phase stabilized pulse to create the method of streak field detection [1,16,76]. Photoelectrons resulting from ionization of a target atom are subjected to a strong near-infrared field, which shifts the electron momenta, streaking the electron velocities as a function of time delay between the two pulses and determining when the electrons are born in the field. In the case of a direct photoionization, the method provides a way to measure the duration of the attosecond pulse. In the case of delayed photoemission, the phase delays give powerful insight into photoemission for different orbitals in atoms or materials. Observed phase delays as short as 10s of attoseconds have been the subject of considerable theoretical investigation to understand the effect of the strong field and other artifacts on the desired interpretations. Similarly, it is possible to use the near-infrared field to detect the timing of the birth of ions by tunnel ionization in a strong field [77]. The timing and direction of a recolliding electron controlled by a strong field, in the very process that is used to produce high harmonics, has resulted in a rich field of investigation [78]. By such experiments, there have been many insights into the re-collision process, the production of high harmonics, and the time scales for the birth of electrons in a strong laser field.

The development of the method of attosecond transient absorption (Fig. 14) provided first measurements of a valence electronic state coherent superposition in ions formed by strong field ionization [79]. The transient absorption technique, importantly, provides a method of general applicability [80]; it can be used to study atoms, molecules, liquids, solids, and plasmas, and available attosecond pulses address the spectral features of

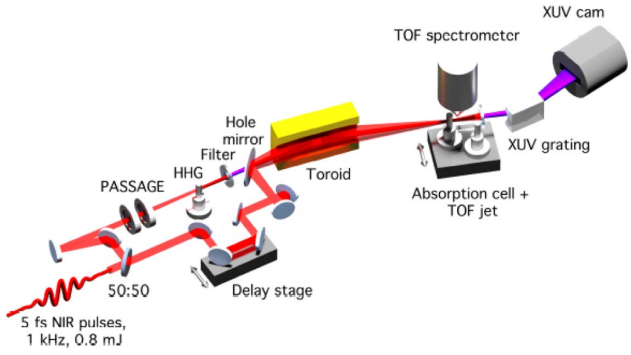

Fig. 14. Setup for attosecond transient absorption, showing a partial polarization gate (PASSAGE) [58].

many elements. The method obtains bonding, oxidation state, and state-resolved information, and it provides powerful details about line shapes, wave packet superpositions, and decays. Because the detection step involves an integration of the total emission from the sample and its interference with the incident extreme ultraviolet attosecond pulse, there is much ongoing theoretical work to ensure that interpretations in the time regime where the near-infrared pulse overlaps with the isolated attosecond pulse can be properly harnessed [81,82].

B. Light-Induced States, Lorentz-to-Fano Line Shapes, Subcycle Interferences, and Wave Packet Superpositions in Atoms and Molecules

Due to the great spectral breadth of isolated attosecond pulses or pulse trains, the pulses are ideally suited to produce massive superpositions of states in atoms or molecules. The excitation can often investigate above or near ionization limits to follow decaying states. The time evolution of the dynamics is obtained by manipulating the initial superposition with few-cycle near-infrared pulses [83]. The near infrared pulses are strong enough to transfer population through other states via lambda (Λ)-, vee (V)-, and ladder (Ξ)-type coupling schemes [84] of two or more near-infrared photons. Many of these have been theoretically described and explored [85]. Moreover, the near-infrared pulses are strong enough to shift levels with the field. These interactions modify the polarization of the medium, which then interferes with the initial attosecond pulse at the detector. The result is a rich detail that can observe light-induced states (coupling to a dark state, which is observed in the attosecond pulse spectrum only during the pulse overlap region) [86] and coherent superpositions or quantum beats (either electronic or vibrational, revealed by lambda- or vee-type coupling through close-lying neighboring states) [87]. Autler–Townes splitting can also be observed if there is a suitable resonance with a neighboring state [88]. The near-infrared field can phase shift the spectral features causing Lorentzian lines to take on a Fano line shape, or vice versa [89], and rapid subcycle oscillations can be observed due to interferences created by ladder-type coupling [90].

Figure 15 demonstrates several of the many kinds of effects observed among the Rydberg states of argon atoms [91]. In the experiment, the extreme ultraviolet attosecond pulse arrives first, and the few-cycle near-infrared pulse modifies the polarization of the medium as a function of time delay. The ionization limit is 15.76 eV, and numerous transient features in states approaching and above the ionization limit are observed. Some time dynamic features in the absorption profiles emerge during the pulse overlap region, including line broadening, sideband structure, subcycle fast modulations, and 5–10 femtosecond slow modulations. There are two general processes underlying the light–matter interaction: energy shifts of individual atomic levels by the strong field and coherent population transfer between atomic eigenstates, revealing the coherent superpositions and other interferences. By combining theories of these two basic processes, excellent descriptions of four main effects labeled in the figure are obtained: (a) broadening and shifting of individual absorption lines at small time delays due to the AC Stark effect; (b) horizontal sideband structures between adjacent absorption resonances at longer time delays due to the AC Stark effect acting on adjacent lines; (c) rapid modulations at 1.3 fs due to ladder-type interferences; and (d) slow modulations at 5–10 fs due to vee-type population transfer, revealing electronic superpositions established by the attosecond pulse.

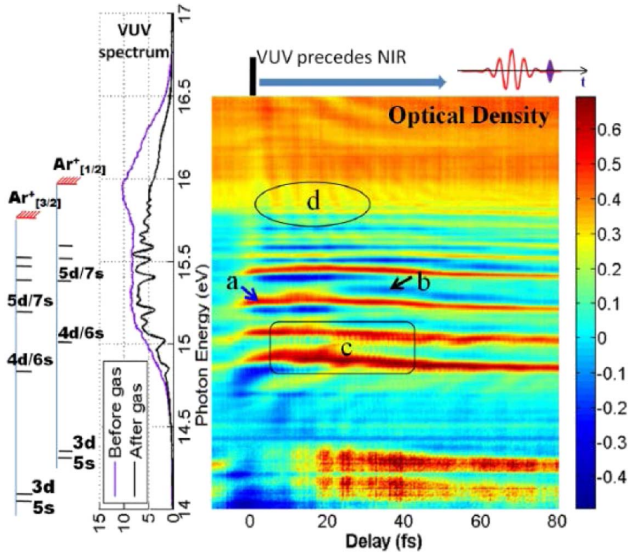

Fig. 15. Attosecond transient absorption spectrum in argon [91]. Static spectrum on left.

C. Atom, Surface, and Nanoparticle Photoelectron Emission

The methods of attosecond streaking and RABBITT (i.e., two-photon sideband interferometry, named by the acronym of the technique, Reconstruction of Attosecond Beating By Interference of Two-photon Transitions) [15] are used to make impressive measurements of the relative phase delays of photoelectron emission from different atoms in mixtures of gases or sequentially in different gases [92,93], in different orbitals within the same atom, or in different band features in photoemission from the surfaces of solid-state materials [94,95]. RABBITT measures the phase delays in sidebands created by the strong field of a near infrared pulse using attosecond pulse trains shifted in time with respect to the near infrared field.

In all cases what is sought is the true Wigner phase delay for the photoemission process [96,97]. The strong field interacting with the sample can perturb the outcome, and there are considerable theoretical discussions about the interpretations of the delays [97]. For example, in Ne atoms, a 21 ± 5 attosecond delay in extreme ultraviolet light photoemission from the 2p orbital, compared to the 2s orbital, is observed experimentally [98]. However, theoretical investigations predict delays half of this value or less [97]. In the process of investigating the phenomena theoretically, it is found that the strong field affects the photoemission delays and this is critical to assess the timing delays. Even with these issues, excellent progress has been made to interpret contributions due to initial-state polarization, final-state interactions of the electron with the final ion state, and Coulomb-laser field coupling in the continuum state. Strong field photoemission has been extended

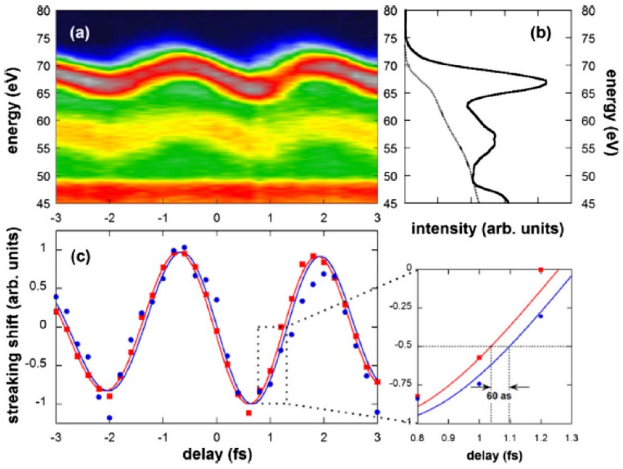

Fig. 16. Streaking delays of the Mg 2p resonance and the first plasmon-like satellite feature in the metal. Reprinted with permission from [94] by the American Physical Society.

to size-selected silicon dioxide nanoparticles [99]. Using carrier-envelope-phase controlled pulses and imaging of the photoelectrons, the results provide clear evidence for the direct ejection and attosecond time scale re-collision dynamics, the effect of local trapping potentials, and the potential application to steering electrons to re-collide with aerosol droplets.

In recent intriguing work on photoemissions from solids, the streaking delays of collective electron oscillations was investigated [94]. In solid magnesium, using an isolated attosecond pulse with a central energy of 118 eV, streaking measurements are performed on both the band feature of the Mg(2p) state, observed at a relative electron kinetic energy of 68 eV (Fig. 16), and the first plasmon-like (plasmon loss) resonance feature at lower kinetic energy (58 eV). The observed 60 as delay of the plasmon feature is interpreted in terms of both the intrinsic plasmon excitation (excited directly by part of the photon energy through interaction of the electron gas with the core hole of the main line) and extrinsic plasmon excitation (excited secondarily by inelastic scattering of the outgoing electron from the main line). With a suitable model for the electron escape and average escape times for the two mechanisms, a finite and distinguishable fraction of the intrinsic plasmon excitation mechanism is determined. The intrinsic process is expected to have considerably shorter electron escape times at higher kinetic energies, allowing a determination of the intrinsic fraction to be 0.1 ± 0.05, even though the extrinsic mechanism dominates.

D. Strong Field Ionization and Charge Migration in Molecules

A rich field of attosecond timing is built around measurements: for example, of the angular clocking of photoelectrons [96], using strong, circularly polarized near-infrared fields to obtain the escape times by electron tunneling from atoms, or attosecond high harmonic interferometry [100]. Moreover, the measurement of state-resolved attosecond transient absorption in strong field ionization provided the first observation of a coherent superposition among valence states of ions produced in

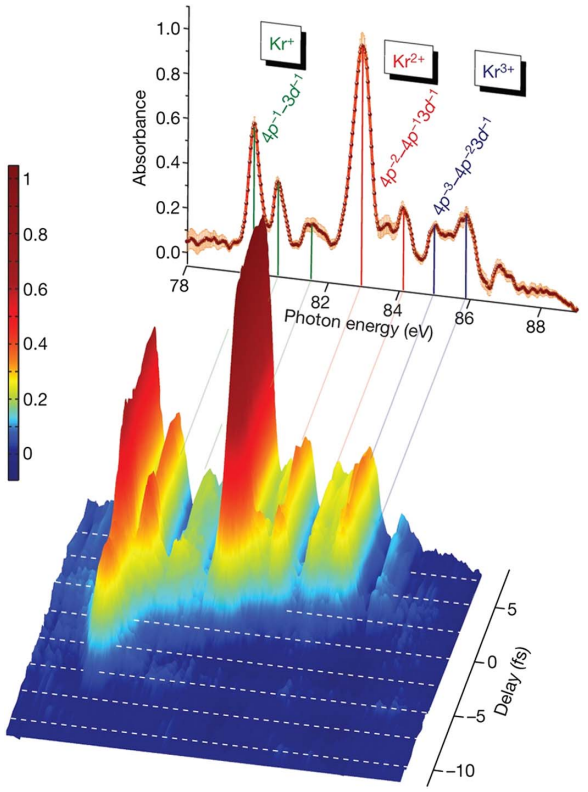

Fig. 17. Transient absorption spectra of krypton in strong field ionization [79].

strong field ionization [79]. In those transient absorption measurements in Kr atoms (Fig. 17), the observed coherent superposition between the $^2P_{1/2}$ and $^2P_{3/2}$ ion states indicates the simultaneous formation of the two electronically excited states in the ion and the preservation of a precise phase relationship between them when they are formed. Moreover, a complete density matrix for the diagonal (population) and off-diagonal (coherence) terms is obtained in an open quantum mechanical system. It was shown theoretically that, if the strong field pulse were longer, the degree of coherence would decrease considerably.

Cederbaum and co-workers [101–104] and Levine and co-workers [105–107] pioneered theoretical analyses of the production and subsequent evolution of coherent superpositions that lead to charge-state dynamics in molecules, i.e., coherent recurrences or charge migration, a holy grail for recent chemical dynamics measurements. Cederbaum and Zobeley [101] calculated that a localized hole created by the removal of an electron from a specific subgroup in a molecule, for example, by an attosecond pulse, could redistribute across the molecule by a correlation-driven process due to a nonstationary state being formed. Subsequent to this seminal work, numerous examples of charge migration dynamics have been assessed theoretically in valence states and inner valence states, including correlated hole and particle dynamics in neutral species [101–107]. These exciting predictions provide strong motivation for experimental groups to observe charge migration and to look for signatures of correlation-driven processes.

In early investigations in the 1990s, it was shown that laser pulses could be used to interrogate charge localization in large molecules by laser dissociation and subsequent mass spectrometric analysis of the ion fragment [108]. This method has recently been applied in an innovative attosecond experiment on gas phase phenylalanine [109]. The attosecond pulse is used to create a sudden hole in the molecule, albeit the pulse is extremely broad (15–35 eV); therefore, the ionization step can, in principle, produce numerous excited states of the phenylalanine ion. A few-cycle near-infrared pulse is then used to fragment the ion by strong field dissociative ionization as a function of time delay, resulting in COOH plus the dication, $C_6H_5CH_2CHNH_2^{++}$ fragment. The dication fragment population exhibits on average a 4.3 fs periodic recurrence that has multiple periods embedded in the signal, which are ascribed to electronic recurrences. Extensive theoretical calculations, coupled with the knowledge that the observed periods are too high to be the frequencies of vibrational recurrences, provides compelling evidence that charge migration is being observed. The long persistence time of the recurrences is intriguing and suggests work on longer time dephasing.

A different kind of charge migration experiment, based on the electron re-collision, high harmonic spectroscopy method, has been performed on the HCCI molecular ion, starting with a strong near-infrared field in the neutral HCCI molecule [110]. By varying the period of the driving laser field, an electron can be sent out from the molecule and timed to re-collide on the time scale of the motion of recurrences of the hole migration in the molecule. Moreover, by aligning the molecules with a separate laser pulse, the recollision dynamics were probed on the next rotational alignment recurrence in a field-free region, allowing side-on versus end-on recollisions. Each harmonic order corresponds to a unique time trajectory for the analysis. Additionally, the phase of each harmonic is measured as a function of alignment angle. The results show that hole migration is occurring by recurrences between the two main electronic states of the ion during the recollision time scale and the re-collisions can be controlled by timing the re-collision trajectory set by the laser wavelength with the hole migration period. The clear evidence for hole migration among the two lowest states of the ion sets a precedent for future investigations of charge migration in molecules and possible correlation-driven charge migration phenomena.

E. Circularly Polarized Attosecond Pulse Phenomena

With the recent demonstrations of circularly polarized high harmonic pulse trains [69,111–113], exciting new work is being done to couple circularly polarized near-infrared driver light with chiral molecules [114]. The small difference in the degree of nonlinearity of the two enantiomers is observed to be greatly amplified in the high harmonic output when using elliptically polarized light fields. Two mechanisms are potentially operating, one involving chiral displacement due to the Lorentz force ($v \times B$), considered to be a weak effect, and another involving dipole excitation of the ion ground state to an excited state, essentially a hole migration driven by the field, resulting in strong changes in the chiral recombination probability, as well as a homodyne enhancement due to underlying nonchiral channels.

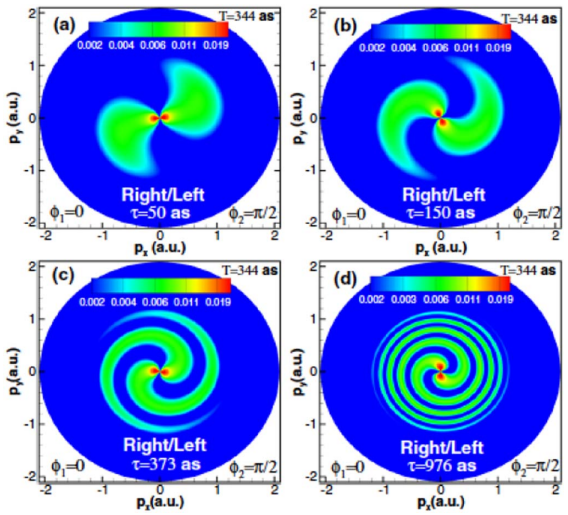

Fig. 18. Predicted helical vortex structures of He photoionization as a function of circularly polarized attosecond pulse delays. Reprinted with permission from [117] by the American Physical Society.

Predictions of methods to create not just circularly polarized attosecond pulse trains but indeed circularly polarized isolated attosecond pulses suggest combinations of fields that can achieve such pulses [115]. Molecular frame photoelectron angular distributions have been theoretically calculated for circularly polarized attosecond pulses and shown to depend on Rabi frequencies with intermediate excited states [116]. Circularly polarized attosecond pulses are theoretically proposed to investigate novel electron phenomena such as electron vortices in photoionization [117]. Subjecting He atoms to two oppositely circularly polarized attosecond pulses is predicted to lead to electron angular distributions in the polarization plane that will exhibit helical vortex structures (Fig. 18).

F. Field-Induced Dielectric Breakdown and Bandgap Semiconductor Dynamics

The application of the method of attosecond transient absorption to solid-state dynamics is emerging as an exciting new field of investigation. In a seminal experiment on a dielectric medium, silicon dioxide, attosecond transient absorption was used to reveal an instantaneous and reversible alteration of the material from an insulator to a conductor through the silicon L edge spectra [118]. There is a transient redshift, due to a dynamic Stark effect, and a large change in the transient absorption in the conduction band of the silicon dioxide, indicative of induced carriers in the conduction band. Concurrent calculations show that the induced polarization of the materials follows the instantaneous field of the driving laser pulse.

In single crystal silicon semiconductor material, electrons were driven by a strong near-infrared field from the valence band to the conduction band via a tunneling process (Fig. 19) [119]. The results reveal a persistent decrease in the conduction band energy, a rapid ponderomotive/Stark effect transient blueshift, and persistent broadening of regions

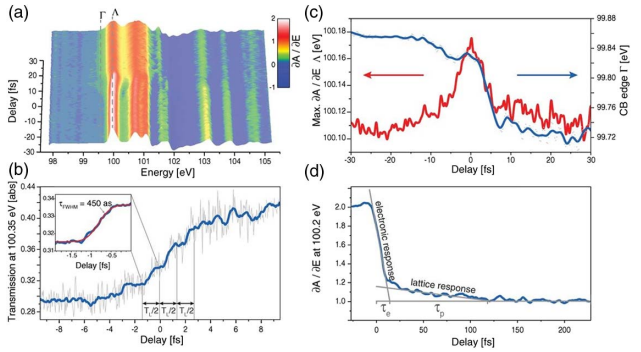

Fig. 19. Silicon attosecond conduction band excitation experiment, showing (a) persistent shifts and broadening and transient shifts in derivative spectra, (b) step-like features in the electronic response, (c) conduction band shift, and (d) slower lattice response. From [119]. Reprinted with permission from AAAS.

within the density of states of the conduction band, all observed through attosecond transient absorption changes on the silicon L edge. An electronic response of less than 450 as is observed, suggesting the response to many-body interactions of electrons and holes when electrons are introduced into the conduction band by the strong near-infrared pulse. On a longer time scale of 60 fs, additional shifts and broadening of the transient features suggest a change in the silicon lattice of 6 pm. The results clearly separate the electronic and nuclear time scales through the experiment.

5. FUTURE PERSPECTIVES

The rapid progress in attosecond optics research is driven by both the needs of scientific applications and advances in driving laser technology. Whereas the new generation driving lasers are being developed at university laboratories worldwide, an international attosecond user facility is being built in Szeged, Hungary, namely, the Extreme Light Infrastructure Attosecond Light Pulse Source (ELI-ALPS). The specifications of the three major driving lasers shown in Fig. 20 are extremely impressive [120]. While being able to deliver few cycle pulses (5 to 10 fs), the repetition of these OPA lasers are 10 to 100 times higher than that of the current lasers of their energy classes (few mJ, 100 mJ and Joule-level), which is beneficial to acquiring data with a high signal-to-noise ratio and optimizing experimental

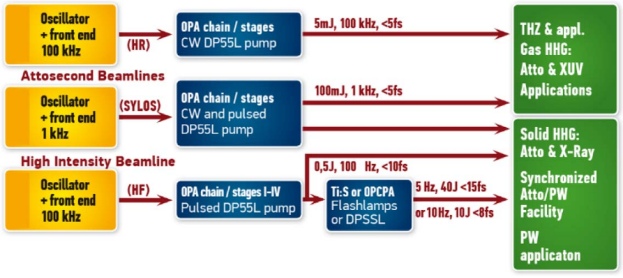

Fig. 20. Driving laser development at the ELI-ALPS [120]. Reprinted with permission.

conditions. The 100 kHz laser is critical for photoelectron spectroscopy experiments to minimize the space charge effects. Attosecond user facilities like this may play important roles because of the high costs of developing and maintain driving lasers with such high average powers.

Projecting forward, the four general directions of laser technology—more energetic pulses, higher average power, longer wavelength drivers, and better control—will continue to define the advances in attosecond technology. Long-wavelength infrared sources have important advantages, and difficulties, for attosecond pulse generation. The advantages are that infrared drivers (1) produce much shorter wavelength attosecond pulses; (2) pulses with much greater bandwidth; and (3) pulses that can also be more background free [121]. These benefits will enable attosecond science to borrow more freely from synchrotron physics, reaching core to valence transitions, for example. It will also allow shorter duration attosecond pulses—in fact, much shorter pulses if investigators can solve how to remove the atto-chirp over such a large bandwidth. It might not even be necessary to remove the chirp to reap the benefit for measurement. A pulse with a known spectral phase can be as useful as one in which the spectral phase is removed [122]. In other words, used correctly, a well-characterized chirped attosecond pulse can be just as valuable as a transform limited pulse. Thus, experiments with very high time resolution—perhaps even approaching the attosecond barrier—are within reach.

There are three difficulties of using long-wavelength drivers for attosecond pulse production. First, the driver is more sensitive to plasma production; therefore, it is more easily chirped and de-focused. This could add to space–time coupling on the attosecond beam emitted from gas cells. Second, the single atom response is weaker for the short-wavelength components of an attosecond pulse. While some of this can be overcome with harmonic gas pressure, it is unclear how close the harmonic generation can come to absorption-limited conversion. Third, short-wavelength pulses will be more difficult to use in pump–probe experiments because of the generally small cross sections for soft x-ray absorption.

Progress will be both in sources and in their application. For soft x-ray attosecond-pump attosecond-probe to be generally applicable low noise attosecond sources are needed, transient grating and related spectroscopies for increased background suppression are needed even more, and excellent focusing must be achieved. The latter is an issue that needs much more attention.

Broadening applications in attosecond science has been slowed by the limited spectral range of attosecond pulses. Thus, it has not been possible to address the spectral features of many important elements, carbon, nitrogen, and oxygen, in attosecond dynamics experiments. This is being resolved by the implementation of long-wavelength driver pulses to generate attosecond pulses from 300–500 eV. In new experiments, it will be possible to investigate carbon nanotubes, graphene, and charge migration dynamics in all-carbon nitrogen–oxygen species, which also opens up all biological systems for study.

Attosecond science has also been limited by the fact that attosecond pulses are weak, and it has not been possible to split an isolated attosecond pulse in two and use one for a pump and one

for the probe. Experiments are therefore forced to couple the isolated attosecond pulse with the strong field of intense near-infrared pulse, which is strong enough to perturb the potentials of the atoms and molecules and affect the outcome of the experiment. In future work, high-flux attosecond pulses will be available to create the pump and probe pulses, operating on x-ray core level transitions, and eliminating the ambiguous regime of pulse overlap. This, however, requires new thinking and spectroscopies on core state spectroscopic transitions and lifetimes.

One key area that will undoubtedly be introduced in the future is multidimensional x-ray spectroscopy [123]. The proposed methods are based on the familiar principles of optical and infrared multidimensional coherent spectroscopies, previously based on magnetic resonance multidimensional methods, but in the unfamiliar spectroscopic regime of x-rays, where core level lifetimes and other features still need to be addressed. When these x-ray techniques are harnessed, there will be many new powerful approaches to investigate dynamics and to peer beneath heterogeneous broadening effects. New applications of attosecond pulses to achieve scientific discoveries will undoubtedly come in the areas of charge migration in molecules and conical intersections [124], and these measurements will be performed by increasingly sophisticated techniques. The emerging use of circularly polarized attosecond pulses will elucidate chiral phenomena in ways not previously anticipated. Novel investigations will explore correlation phenomena in materials such as insulator to metal transitions and superconductivity. A large area of x-ray attosecond spectroscopic investigations will involve charge transfer and charge transport in transition metal solar photovoltaic systems, fuel cells, and high-speed detectors. There is great promise for understanding and implementing electronic and optical signal processing for enhanced speeds in the near future with attosecond technologies [125].

Funding. Defense Advanced Research Projects Agency (DARPA) (W31P4Q1310017); Army Research Office (ARO) (WN911NF-14-1-0383); Air Force Office of Scientific Research (AFOSR) (FA9550-13-1-0010, FA9550-15-1-0037, FA9550-16-1-0013); National Science Foundation (NSF) (CHE-1361226, PHY-1506345); National Research Council Canada (NRC); Natural Sciences and Engineering Research Council of Canada (NSERC); Canada Research Chairs; Canada Foundation for Innovation (CFI) (203614); Ontario Research Fund (21240); U.S. Department of Energy (DOE) (DE-AC03-76SF00); W.M. Keck Foundation; National Security Science and Engineering Faculty Fellowship (NSSEFF) (FA9550-10-1-0195).

REFERENCES

1. F. Krausz and M. Ivanov, "Attosecond physics," Rev. Mod. Phys. **81**, 163–234 (2009).
2. M. Chini, K. Zhao, and Z. Chang, "The generation, characterization and applications of broadband isolated attosecond pulses," Nat. Photonics **8**, 178–186 (2014).
3. Z. Chang, *Fundamentals of Attosecond Optics* (CRC Press, 2011), Vol. **1**.
4. A. McPherson, G. Gibson, H. Jara, U. Johann, T. S. Luk, I. McIntyre, K. Boyer, and C. K. Rhodes, "Studies of multiphoton production of vacuum-ultraviolet radiation in the rare gases," J. Opt. Soc. Am. B **4**, 595–601 (1987).
5. M. Ferray, A. l'Huillier, X. Li, L. Lompre, G. Mainfray, and C. Manus, "Multiple-harmonic conversion of 1064 nm radiation in rare gases," J. Phys. B **21**, L31–L35 (1988).
6. P. B. Corkum, "Plasma perspective on strong field multiphoton ionization," Phys. Rev. Lett. **71**, 1994–1997 (1993).
7. K. Schafer, B. Yang, L. DiMauro, and K. Kulander, "Above threshold ionization beyond the high harmonic cutoff," Phys. Rev. Lett. **70**, 1599–1602 (1993).
8. M. Lewenstein, P. Balcou, M. Y. Ivanov, A. L'huillier, and P. B. Corkum, "Theory of high-harmonic generation by low-frequency laser fields," Phys. Rev. A **49**, 2117–2132 (1994).
9. W. Becker, S. Long, and J. McIver, "Modeling harmonic generation by a zero-range potential," Phys. Rev. A **50**, 1540–1560 (1994).
10. P. Antoine, A. L'huillier, and M. Lewenstein, "Attosecond pulse trains using high-order harmonics," Phys. Rev. Lett. **77**, 1234–1237 (1996).
11. J. J. Macklin, J. Kmetec, and C. Gordon III, "High-order harmonic generation using intense femtosecond pulses," Phys. Rev. Lett. **70**, 766–769 (1993).
12. E. Constant, D. Garzella, P. Breger, E. Mével, C. Dorrer, C. Le Blanc, F. Salin, and P. Agostini, "Optimizing high harmonic generation in absorbing gases: model and experiment," Phys. Rev. Lett. **82**, 1668–1671 (1999).
13. P. Salieres, A. L'Huillier, and M. Lewenstein, "Coherence control of high-order harmonics," Phys. Rev. Lett. **74**, 3776–3779 (1995).
14. A. Rundquist, C. G. Durfee, Z. H. Chang, C. Herne, S. Backus, M. M. Murnane, and H. C. Kapteyn, "Phase-matched generation of coherent soft X-rays," Science **280**, 1412–1415 (1998).
15. P. M. Paul, E. Toma, P. Breger, G. Mullot, F. Augé, P. Balcou, H. Muller, and P. Agostini, "Observation of a train of attosecond pulses from high harmonic generation," Science **292**, 1689–1692 (2001).
16. M. Hentschel, R. Kienberger, C. Spielmann, G. Reider, N. Milosevic, T. Brabec, P. Corkum, U. Heinzmann, M. Drescher, and F. Krausz, "Attosecond metrology," Nature **414**, 509–513 (2001).
17. G. Sansone, L. Poletto, and M. Nisoli, "High-energy attosecond light sources," Nat. Photonics **5**, 655–663 (2011).
18. K. Zhao, Q. Zhang, M. Chini, Y. Wu, X. Wang, and Z. Chang, "Tailoring a 67 attosecond pulse through advantageous phase-mismatch," Opt. Lett. **37**, 3891–3893 (2012).
19. Y. Mairesse and F. Quéré, "Frequency-resolved optical gating for complete reconstruction of attosecond bursts," Phys. Rev. A **71**, 011401 (2005).
20. M. Chini, S. Gilbertson, S. D. Khan, and Z. Chang, "Characterizing ultrabroadband attosecond lasers," Opt. Express **18**, 13006–13016 (2010).
21. S. Ghimire, A. D. DiChiara, E. Sistrunk, P. Agostini, L. F. DiMauro, and D. A. Reis, "Observation of high-order harmonic generation in a bulk crystal," Nat. Phys. **7**, 138–141 (2010).
22. S. R. Leone, C. W. McCurdy, J. Burgdorfer, L. S. Cederbaum, Z. Chang, N. Dudovich, J. Feist, C. H. Greene, M. Ivanov, R. Kienberger, U. Keller, M. F. Kling, Z.-H. Loh, T. Pfeifer, A. N. Pfeiffer, R. Santra, K. Schafer, A. Stolow, U. Thumm, and M. J. J. Vrakking, "What will it take to observe processes in "real time"?" Nat. Photonics **8**, 162–166 (2014).
23. A. Rundquist, C. Durfee, Z. Chang, G. Taft, E. Zeek, S. Backus, M. Murnane, H. Kapteyn, I. Christov, and V. Stoev, "Ultrafast laser and amplifier sources," Appl. Phys. B **65**, 161–174 (1997).
24. S. Gilbertson, H. Mashiko, C. Li, E. Moon, and Z. Chang, "Effects of laser pulse duration on extreme ultraviolet spectra from double optical gating," Appl. Phys. Lett. **93**, 111105 (2008).
25. H. Mashiko, C. M. Nakamura, C. Li, E. Moon, H. Wang, J. Tackett, and Z. Chang, "Carrier-envelope phase stabilized 5.6 fs, 1.2 mJ pulses," Appl. Phys. Lett. **90**, 161114 (2007).
26. D. J. Jones, S. A. Diddams, J. K. Ranka, A. Stentz, R. S. Windeler, J. L. Hall, and S. T. Cundiff, "Carrier-envelope phase control of femtosecond mode-locked lasers and direct optical frequency synthesis," Science **288**, 635–639 (2000).
27. C. Li, E. Moon, and Z. Chang, "Carrier-envelope phase shift caused by variation of grating separation," Opt. Lett. **31**, 3113–3115 (2006).

28. C. Li, E. Moon, H. Mashiko, C. M. Nakamura, P. Ranitovic, C. M. Maharjan, C. L. Cocke, Z. Chang, and G. G. Paulus, "Precision control of carrier-envelope phase in grating based chirped pulse amplifiers," Opt. Express **14**, 11468–11476 (2006).
29. I. F. Barna, J. Wang, and J. Burgdörfer, "Angular distribution in two-photon double ionization of helium by intense attosecond soft-x-ray pulses," Phys. Rev. A **73**, 023402 (2006).
30. H. Hasegawa, E. J. Takahashi, Y. Nabekawa, K. L. Ishikawa, and K. Midorikawa, "Multiphoton ionization of He by using intense high-order harmonics in the soft-x-ray region," Phys. Rev. A **71**, 023407 (2005).
31. E. Cunningham, *Towards High-flux Isolated Attosecond Pulses with A 200 TW CPA* (University of Central Florida Orlando, 2015).
32. E. J. Takahashi, P. Lan, O. D. Mücke, Y. Nabekawa, and K. Midorikawa, "Attosecond nonlinear optics using gigawatt-scale isolated attosecond pulses," Nat. Commun. **4**, 2691 (2013).
33. E. Cunningham, Y. Wu, and Z. Chang, "Carrier-envelope phase control of a 10 Hz, 25 TW laser for high-flux extreme ultraviolet quasi-continuum generation," Appl. Phys. Lett. **107**, 201108 (2015).
34. Y. Wu, E. Cunningham, H. Zang, J. Li, M. Chini, X. Wang, Y. Wang, K. Zhao, and Z. Chang, "Generation of high-flux attosecond extreme ultraviolet continuum with a 10 TW laser," Appl. Phys. Lett. **102**, 201104 (2013).
35. X. Feng, S. Gilbertson, H. Mashiko, H. Wang, S. D. Khan, M. Chini, Y. Wu, K. Zhao, and Z. Chang, "Generation of isolated attosecond pulses with 20 to 28 femtosecond lasers," Phys. Rev. Lett. **103**, 183901 (2009).
36. F. Tavella, Y. Nomura, L. Veisz, V. Pervak, A. Marcinkevičius, and F. Krausz, "Dispersion management for a sub-10-fs, 10 TW optical parametric chirped-pulse amplifier," Opt. Lett. **32**, 2227–2229 (2007).
37. H. Mashiko, S. Gilbertson, M. Chini, X. Feng, C. Yun, H. Wang, S. D. Khan, S. Chen, and Z. Chang, "Extreme ultraviolet supercontinua supporting pulse durations of less than one atomic unit of time," Opt. Lett. **34**, 3337–3339 (2009).
38. B. Shan and Z. Chang, "Dramatic extension of the high-order harmonic cutoff by using a long-wavelength driving field," Phys. Rev. A **65**, 011804 (2001).
39. Z. Chang, A. Rundquist, H. Wang, M. M. Murnane, and H. C. Kapteyn, "Generation of coherent soft X rays at 2.7 nm using high harmonics," Phys. Rev. Lett. **79**, 2967–2970 (1997).
40. B. E. Schmidt, A. D. Shiner, M. Giguère, P. Lassonde, C. A. Trallero-Herrero, J. Kieffer, P. Corkum, D. Villeneuve, and F. Légaré, "High harmonic generation with long-wavelength few-cycle laser pulses," J. Phys. B **45**, 074008 (2012).
41. S. Cousin, F. Silva, S. Teichmann, M. Hemmer, B. Buades, and J. Biegert, "High-flux table–top soft x-ray source driven by sub-2-cycle, CEP stable, 1.85-μm 1-kHz pulses for carbon K-edge spectroscopy," Opt. Lett. **39**, 5383–5386 (2014).
42. F. Silva, S. M. Teichmann, S. L. Cousin, M. Hemmer, and J. Biegert, "Spatiotemporal isolation of attosecond soft X-ray pulses in the water window," Nat. Commun. **6**, 6611 (2015).
43. N. Ishii, K. Kaneshima, K. Kitano, T. Kanai, S. Watanabe, and J. Itatani, "Carrier-envelope phase-dependent high harmonic generation in the water window using few-cycle infrared pulses," Nat. Commun. **5**, 3331 (2014).
44. N. Ishii, K. Kaneshima, T. Kanai, S. Watanabe, and J. Itatani, "Sub-two-cycle millijoule optical pulses at 1600 nm from a BiB_3O_6 optical parametric chirped-pulse amplifier," in *CLEO: Science and Innovations* (Optical Society of America, 2015), paper SF1M.3.
45. Y. Yin, J. Li, X. Ren, K. Zhao, Y. Wu, E. Cunningham, and Z. Chang, "High-efficiency optical parametric chirped-pulse amplifier in BiB_3O_6 for generation of 3 mJ, two-cycle, carrier-envelope-phase-stable pulses at 1.7 μm," Opt. Lett. **41**, 1142–1145 (2016).
46. K.-H. Hong, C.-J. Lai, J. P. Siqueira, P. Krogen, J. Moses, C.-L. Chang, G. J. Stein, L. E. Zapata, and F. X. Kärtner, "Multi-mJ, kHz, 2.1 μm optical parametric chirped-pulse amplifier and high-flux soft x-ray high-harmonic generation," Opt. Lett. **39**, 3145–3148 (2014).
47. Y. Deng, A. Schwarz, H. Fattahi, M. Ueffing, X. Gu, M. Ossiander, T. Metzger, V. Pervak, H. Ishizuki, T. Taira, T. Kobayashi, G. Marcus, F. Krausz, R. Kienberger, and N. Karpowicz, "Carrier-envelope-phase-stable, 1.2 mJ, 1.5 cycle laser pulses at 2.1 μm," Opt. Lett. **37**, 4973–4975 (2012).
48. T. Popmintchev, M.-C. Chen, D. Popmintchev, P. Arpin, S. Brown, S. Ališauskas, G. Andriukaitis, T. Balčiunas, O. D. Mücke, A. Pugzlys, A. Baltuška, B. Shim, S. E. Schrauth, A. Gaeta, C. Hernández-García, L. Plaja, A. Becker, A. Jaron-Becker, M. M. Murnane, and H. C. Kapteyn, "Bright coherent ultrahigh harmonics in the keV X-ray regime from mid-infrared femtosecond lasers," Science **336**, 1287–1291 (2012).
49. J. Itatani, D. Zeidler, J. Levesque, M. Spanner, D. Villeneuve, and P. Corkum, "Controlling high harmonic generation with molecular wave packets," Phys. Rev. Lett. **94**, 123902 (2005).
50. G. Vampa, T. Hammond, N. Thiré, B. Schmidt, F. Légaré, C. McDonald, T. Brabec, and P. Corkum, "Linking high harmonics from gases and solids," Nature **522**, 462–464 (2015).
51. M. Hohenleutner, F. Langer, O. Schubert, M. Knorr, U. Huttner, S. Koch, M. Kira, and R. Huber, "Real-time observation of interfering crystal electronics in high-harmonic Generation," Nature **523**, 572–575 (2015).
52. T. Luu, M. Garg, S. Y. Kruchinin, A. Moulet, M. T. Hassan, and E. Goulielmakis, "Extreme ultraviolet high-harmonic spectroscopy of solids," Nature **521**, 498–502 (2015).
53. K. T. Kim, C. M. Kim, M.-G. Baik, G. Umesh, and C. H. Nam, "Single sub–50–attosecond pulse generation from chirp-compensated harmonic radiation using material dispersion," Phys. Rev. A **69**, 051805 (2004).
54. J. Tate, T. Auguste, H. Muller, P. Salieres, P. Agostini, and L. DiMauro, "Scaling of wave-packet dynamics in an intense midinfrared field," Phys. Rev. Lett. **98**, 013901 (2007).
55. P. Corkum, N. Burnett, and M. Y. Ivanov, "Subfemtosecond pulses," Opt. Lett. **19**, 1870–1872 (1994).
56. B. Shan, S. Ghimire, and Z. Chang, "Generation of the attosecond extreme ultraviolet supercontinuum by a polarization gating," J. Mod. Opt. **52**, 277–283 (2005).
57. H. Mashiko, S. Gilbertson, C. Li, S. D. Khan, M. M. Shakya, E. Moon, and Z. Chang, "Double optical gating of high-order harmonic generation with carrier-envelope phase stabilized lasers," Phys. Rev. Lett. **100**, 103906 (2008).
58. H. Timmers, M. Sabbar, J. Hellwagner, D. M. Neumark, and S. R. Leone, "Polarization assisted amplitude gating as a route to tunable, high-contrast attosecond pulses" (submitted).
59. K. T. Kim, C. Zhang, T. Ruchon, J.-F. Hergott, T. Auguste, D. Villeneuve, P. Corkum, and F. Quéré, "Photonic streaking of attosecond pulse trains," Nat. Photonics **7**, 651–656 (2013).
60. H. Vincenti, A. Borot, T. Hammond, K. T. Kim, J. Wheeler, C. Zhang, T. Ruchon, T. Auguste, J. Hergott, and D. Villeneuve, "Applications of ultrafast wavefront rotation in highly nonlinear optics," J. Phys. B **47**, 124004 (2014).
61. M. Ivanov, P. Corkum, T. Zuo, and A. Bandrauk, "Routes to control of intense-field atomic polarizability," Phys. Rev. Lett. **74**, 2933–2936 (1995).
62. M. Drescher, M. Hentschel, R. Kienberger, G. Tempea, C. Spielmann, G. A. Reider, P. B. Corkum, and F. Krausz, "X-ray pulses approaching the attosecond frontier," Science **291**, 1923–1927 (2001).
63. J. Itatani, F. Quéré, G. L. Yudin, M. Y. Ivanov, F. Krausz, and P. B. Corkum, "Attosecond streak camera," Phys. Rev. Lett. **88**, 173903 (2002).
64. K. T. Kim, D. Villeneuve, and P. Corkum, "Manipulating quantum paths for novel attosecond measurement methods," Nat. Photonics **8**, 187–194 (2014).
65. K. T. Kim, C. Zhang, A. D. Shiner, S. E. Kirkwood, E. Frumker, G. Gariepy, A. Naumov, D. Villeneuve, and P. Corkum, "Manipulation of quantum paths for space-time characterization of attosecond pulses," Nat. Phys. **9**, 159–163 (2013).
66. D. H. Ko and P. B. Corkum, "All-optical single-shot measurement of time-dependent fields in short pulses," paper #2, Atto2015, July 6-10, 2015 in Saint-Sauveur, Québec, Canada.
67. K. T. Kim, C. Zhang, A. D. Shiner, B. E. Schmidt, F. Légaré, D. Villeneuve, and P. Corkum, "Petahertz optical oscilloscope," Nat. Photonics **7**, 958–962 (2013).

68. H. Zhang, C. Jing, J. Yao, G. Li, B. Zeng, W. Chu, J. Ni, H. Xie, H. Xu, and S. L. Chin, "Rotational coherence encoded in an "air-laser" spectrum of nitrogen molecular ions in an intense laser field," Phys. Rev. X **3**, 041009 (2013).
69. A. Fleischer, O. Kfir, T. Diskin, P. Sidorenko, and O. Cohen, "Spin angular momentum and tunable polarization in high-harmonic generation," Nat. Photonics **8**, 543–549 (2014).
70. G. Gariepy, J. Leach, K. T. Kim, T. J. Hammond, E. Frumker, R. W. Boyd, and P. B. Corkum, "Creating high-harmonic beams with controlled orbital angular momentum," Phys. Rev. Lett. **113**, 153901 (2014).
71. M. Zürch, C. Kern, P. Hansinger, A. Dreischuh, and C. Spielmann, "Strong-field physics with singular light beams," Nat. Phys. **8**, 743–746 (2012).
72. C. Hernández-García, A. Picón, J. San Román, and L. Plaja, "Attosecond extreme ultraviolet vortices from high-order harmonic generation," Phys. Rev. Lett. **111**, 083602 (2013).
73. Z. Li, G. Brown, and P. B. Corkum, "All-optical phase zone plate for high harmonic generation," P1-14 Atto2015, July 6-10, 2015 in Saint-Sauveur, Québec, Canada.
74. H. Worner, J. Bertrand, D. Kartashov, P. Corkum, and D. Villeneuve, "Following a chemical reaction using high-harmonic spectroscope," Nature **466**, 604–607 (2010).
75. H. Wörner, J. Bertrand, B. Fabre, J. Higuet, H. Ruf, A. Dubrouil, S. Patchkovskii, M. Spanner, Y. Mairesse, and V. Blanchet, "Conical intersection dynamics in NO_2 probed by homodyne high-harmonic spectroscopy," Science **334**, 208–212 (2011).
76. M. Drescher, M. Hentschel, R. Kienberger, M. Uiberacker, V. Yakovlev, A. Scrinzi, T. Westerwalbesloh, U. Kleineberg, U. Heinzmann, and F. Krausz, "Time-resolved atomic inner-shell spectroscopy," Nature **419**, 803–807 (2002).
77. M. Uiberacker, T. Uphues, M. Schultze, A. J. Verhoef, V. Yakovlev, M. F. Kling, J. Rauschenberger, N. M. Kabachnik, H. Schröder, and M. Lezius, "Attosecond real-time observation of electron tunnelling in atoms," Nature **446**, 627–632 (2007).
78. S. Haessler, J. Caillat, and P. Salières, "Self-probing of molecules with high harmonic generation," J. Phys. B **44**, 203001 (2011).
79. E. Goulielmakis, Z.-H. Loh, A. Wirth, R. Santra, N. Rohringer, V. S. Yakovlev, S. Zherebtsov, T. Pfeifer, A. M. Azzeer, M. F. Kling, S. R. Leone, and F. Krausz, "Real-time observation of valence electron motion," Nature **466**, 739–743 (2010).
80. M. Chini, H. Wang, B. Zhao, Y. Cheng, S. Chen, Y. Wu, and Z. Chang, "Attosecond absorption spectroscopy," in *Progress in Ultrafast Intense Laser Science* (Springer, 2013), pp. 135–150.
81. R. Santra, V. S. Yakovlev, T. Pfeifer, and Z.-H. Loh, "Theory of attosecond transient absorption spectroscopy of strong-field-generated ions," Phys. Rev. A **83**, 033405 (2011).
82. S. Pabst, A. Sytcheva, A. Moulet, A. Wirth, E. Goulielmakis, and R. Santra, "Theory of attosecond transient-absorption spectroscopy of krypton for overlapping pump and probe pulses," Phys. Rev. A **86**, 063411 (2012).
83. A. R. Beck, D. M. Neumark, and S. R. Leone, "Probing ultrafast dynamics with attosecond transient absorption," Chem. Phys. Lett. **624**, 119–130 (2015).
84. M. Fleischhauer, A. Imamoglu, and J. P. Marangos, "Electromagnetically induced transparency: optics in coherent media," Rev. Mod. Phys. **77**, 633–673 (2005).
85. S. Chen, M. Wu, M. B. Gaarde, and K. J. Schafer, "Quantum interference in attosecond transient absorption of laser-dressed helium atoms," Phys. Rev. A **87**, 033408 (2013).
86. S. Chen, M. J. Bell, A. R. Beck, H. Mashiko, M. Wu, A. N. Pfeiffer, M. B. Gaarde, D. M. Neumark, S. R. Leone, and K. J. Schafer, "Light-induced states in attosecond transient absorption spectra of laser-dressed helium," Phys. Rev. A **86**, 063408 (2012).
87. A. R. Beck, B. Bernhardt, E. R. Warrick, M. Wu, S. Chen, M. B. Gaarde, K. J. Schafer, D. M. Neumark, and S. R. Leone, "Attosecond transient absorption probing of electronic superpositions of bound states in neon: detection of quantum beats," New J. Phys. **16**, 113016 (2014).
88. M. Wu, S. Chen, M. B. Gaarde, and K. J. Schafer, "Time-domain perspective on Autler-Townes splitting in attosecond transient absorption of laser-dressed helium atoms," Phys. Rev. A **88**, 043416 (2013).
89. C. Ott, A. Kaldun, P. Raith, K. Meyer, M. Laux, J. Evers, C. H. Keitel, C. H. Greene, and T. Pfeifer, "Lorentz meets Fano in spectral line shapes: a universal phase and its laser control," Science **340**, 716–720 (2013).
90. M. Chini, X. Wang, Y. Cheng, Y. Wu, D. Zhao, D. A. Telnov, S.-I. Chu, and Z. Chang, "Sub-cycle oscillations in virtual states brought to light," Sci. Rep. **3**, 1105 (2013).
91. W. Cao, E. R. Warrick, D. M. Neumark, and S. R. Leone, "Attosecond transient absorption of argon atoms in the vacuum ultraviolet region: line energy shifts versus coherent population transfer," New J. Phys. **18**, 013041 (2016).
92. C. Cirelli, M. Sabbar, S. Heuser, R. Boge, M. Lucchini, L. Gallmann, and U. Keller, "Energy dependent photoemission time delays of noble gas atoms using coincidence attosecond streaking," IEEE J. Sel. Top. Quantum Electron. **21**, 1–7 (2015).
93. C. Palatchi, J. M. Dahlström, A. Kheifets, I. Ivanov, D. Canaday, P. Agostini, and L. DiMauro, "Atomic delay in helium, neon, argon and krypton," J. Phys. B **47**, 245003 (2014).
94. C. Lemell, S. Neppl, G. Wachter, K. Tőkési, R. Ernstorfer, P. Feulner, R. Kienberger, and J. Burgdörfer, "Real-time observation of collective excitations in photoemission," Phys. Rev. B **91**, 241101 (2015).
95. R. Locher, L. Castiglioni, M. Lucchini, M. Greif, L. Gallmann, J. Osterwalder, M. Hengsberger, and U. Keller, "Energy-dependent photoemission delays from noble metal surfaces by attosecond interferometry," optica **2**, 405–410 (2015).
96. A. S. Landsman and U. Keller, "Attosecond science and the tunnelling time problem," Phys. Rep. **547**, 1–24 (2015).
97. R. Pazourek, S. Nagele, and J. Burgdörfer, "Attosecond chronoscopy of photoemission," Rev. Mod. Phys. **87**, 765–802 (2015).
98. M. Schultze, M. Fieß, N. Karpowicz, J. Gagnon, M. Korbman, M. Hofstetter, S. Neppl, A. Cavalieri, Y. Komninos, and T. Mercouris, "Delay in photoemission," Science **328**, 1658–1662 (2010).
99. F. Suszmann, L. Seiffert, S. Zherebtsov, V. Mondes, J. Stierle, M. Arbeiter, J. Plenge, P. Rupp, C. Peltz, A. Kessel, S. A. Trushin, B. Ahn, D. Kim, C. Graf, E. Ruhl, M. F. Kling, and T. Fennel, "Field propagation-induced directionality of carrier-envelope phase-controlled photoemission from nanospheres," Nat. Commun. **6**, 7944 (2015).
100. O. Pedatzur, G. Orenstein, V. Serbinenko, H. Soifer, B. D. Bruner, A. J. Uzan, D. S. Brambila, A. G. Harvey, L. Torlina, F. Morales, O. Smirnova, and N. Dudovich, "Attosecond tunnelling interferometry," Nat. Phys. **11**, 815–819 (2015).
101. L. S. Cederbaum and J. Zobeley, "Ultrafast charge migration by electron correlation," Chem. Phys. Lett. **307**, 205–210 (1999).
102. A. I. Kuleff, S. Lünnemann, and L. S. Cederbaum, "Ultrafast charge migration following valence ionization of 4-methylphenol: jumping over the aromatic ring," J. Phys. Chem. A **114**, 8676–8679 (2010).
103. A. D. Dutoi, M. Wormit, and L. S. Cederbaum, "Ultrafast charge separation driven by differential particle and hole mobilities," J. Chem. Phys. **134**, 024303 (2011).
104. A. I. Kuleff and L. S. Cederbaum, "Ultrafast correlation-driven electron dynamics," J. Phys. B **47**, 124002 (2014).
105. F. Remacle, R. Levine, E. Schlag, and R. Weinkauf, "Electronic control of site selective reactivity: a model combining charge migration and dissociation," J. Phys. Chem. A **103**, 10149–10158 (1999).
106. F. Remacle and R. D. Levine, "An electronic time scale in chemistry," Proc. Natl. Acad. Sci. USA **103**, 6793–6798 (2006).
107. B. Mignolet, R. Levine, and F. Remacle, "Control of electronic dynamics visualized by angularly resolved photoelectron spectra: A dynamical simulation with an IR pump and XUV attosecond-pulse-train probe," Phys. Rev. A **89**, 021403 (2014).
108. R. Weinkauf, P. Schanen, D. Yang, S. Soukara, and E. Schlag, "Elementary processes in peptides: electron mobility and dissociation in peptide cations in the gas phase," J. Phys. Chem. **99**, 11255–11265 (1995).
109. F. Calegari, D. Ayuso, A. Trabattoni, L. Belshaw, S. De Camillis, S. Anumula, F. Frassetto, L. Poletto, A. Palacios, and P. Decleva, "Ultrafast electron dynamics in phenylalanine initiated by attosecond pulses," Science **346**, 336–339 (2014).

110. P. Kraus, B. Mignolet, D. Baykusheva, A. Rupenyan, L. Horný, E. Penka, G. Grassi, O. Tolstikhin, J. Schneider, and F. Jensen, "Measurement and laser control of attosecond charge migration in ionized iodoacetylene," Science **350**, 790–795 (2015).
111. O. Kfir, P. Grychtol, E. Turgut, R. Knut, D. Zusin, D. Popmintchev, T. Popmintchev, H. Nembach, J. M. Shaw, and A. Fleischer, "Generation of bright phase-matched circularly-polarized extreme ultraviolet high harmonics," Nat. Photonics **9**, 99–105 (2014).
112. D. D. Hickstein, F. J. Dollar, P. Grychtol, J. L. Ellis, R. Knut, C. Hernández-García, D. Zusin, C. Gentry, J. M. Shaw, T. Fan, K. M. Dorney, A. Becker, A. Jaroń-Becker, H. C. Kapteyn, M. M. Murnane, and C. G. Durfee, "Non-collinear generation of angularly isolated circularly polarized high harmonics," Nat. Photonics **9**, 743–750 (2015).
113. T. Fan, P. Grychtol, R. Knut, C. Hernández-García, D. D. Hickstein, D. Zusin, C. Gentry, F. J. Dollar, C. A. Mancuso, C. W. Hogle, O. Kfir, D. Legut, K. Carva, J. L. Ellis, K. M. Dorney, C. Chen, O. G. Shpyrko, E. E. Fullerton, O. Cohen, P. M. Oppeneer, D. B. Milošević, A. Becker, A. A. Jaroń-Becker, T. Popmintchev, M. M. Murnane, and H. C. Kapteyn, "Bright circularly polarized soft x-ray high harmonics for x-ray magnetic circular dichroism," Proc. Natl. Acad. Sci. USA **112**, 14206–14211 (2015).
114. R. Cireasa, A. Boguslavskiy, B. Pons, M. Wong, D. Descamps, S. Petit, H. Ruf, N. Thiré, A. Ferré, and J. Suarez, "Probing molecular chirality on a sub-femtosecond timescale," Nat. Phys. **11**, 654–658 (2015).
115. K.-J. Yuan and A. D. Bandrauk, "Circularly polarized molecular high-order harmonic generation in H 2+ with intense laser pulses and static fields," Phys. Rev. A **83**, 063422 (2011).
116. K.-J. Yuan, S. Chelkowski, and A. D. Bandrauk, "Molecular photoelectron angular distribution rotations in multi-photon resonant ionization of H2+ by circularly polarized ultraviolet laser pulses," J. Chem. Phys. **142**, 144304 (2015).
117. J. N. Djiokap, S. Hu, L. Madsen, N. Manakov, A. Meremianin, and A. F. Starace, "Electron vortices in photoionization by circularly polarized attosecond pulses," Phys. Rev. Lett. **115**, 113004 (2015).
118. M. Schultze, E. M. Bothschafter, A. Sommer, S. Holzner, W. Schweinberger, M. Fiess, M. Hofstetter, R. Kienberger, V. Apalkov, V. S. Yakovlev, M. I. Stockman, and F. Krausz, "Controlling dielectrics with the electric field of light," Nature **493**, 75–78 (2012).
119. M. Schultze, K. Ramasesha, C. Pemmaraju, S. Sato, D. Whitmore, A. Gandman, J. S. Prell, L. Borja, D. Prendergast, K. Yabana, D. M. Neumark, and S. R. Leone, "Attosecond band-gap dynamics in silicon," Science **346**, 1348–1352 (2014).
120. http://www.eli-hu.hu/?q=en/02_Parameters.
121. C. Zhang, G. Vampa, D. Villeneuve, and P. Corkum, "Attosecond lighthouse driven by sub-two-cycle, 1.8 μm laser pulses," J. Phys. B **48**, 061001 (2015).
122. G. Yudin, A. Bandrauk, and P. Corkum, "Chirped attosecond photoelectron spectroscopy," Phys. Rev. Lett. **96**, 063002 (2006).
123. S. Mukamel, D. Healion, Y. Zhang, and J. D. Biggs, "Multidimensional attosecond resonant X-ray spectroscopy of molecules: Lessons from the optical regime," Ann. Rev. Phys. Chem. **64**, 101–127 (2013).
124. M. Kowalewski, K. Bennett, K. E. Dorfman, and S. Mukamel, "Catching conical intersections in the act: monitoring transient electronic coherences by attosecond stimulated x-ray Raman signals," Phys. Rev. Lett. **115**, 193003 (2015).
125. F. Krausz and M. I. Stockman, "Attosecond metrology: from electron capture to future signal processing," Nat. Photonics **8**, 205–213 (2014).